Journal of Geophysical Research: Solid Earth

Supporting Information for

Contrasting Mesozoic evolution across the boundary between on and off craton regions of the South African plateau inferred from apatite fission track and (U-Th-Sm)/He thermochronology

Mark Wildman[1], Roderick Brown[1], Cristina Persano[1], Romain Beucher[1]*, Finlay M. Stuart[2], Vhairi Mackintosh[3], Kerry Gallagher[4], James Schwanethal[5] and Andrew Carter[6]

1. School of Geographical and Earth Sciences, College of Science and Engineering, University of Glasgow, Gregory Building, Glasgow, G12 8QQ, Scotland.

2. Scottish Universities Environmental Research Centre, Rankine Avenue, Scottish Enterprise Technology Park, East Kilbride, G75 0QF, UK

3. School of Earth Sciences, University of Melbourne, Melbourne, Victoria, Australia

4. Géosciences Rennes, Université de Rennes 1, Campus de Beaulieu, 35042 Rennes, France

5. Department of Earth Sciences, University College London, Gower Street, London, WC1E 6BT

6. Department of Earth and Planetary Sciences, Birkbeck, University of London, Malet Street, WC1E 7HX, United Kingdom

* Current address: Department of Earth Science, Faculty of Mathematics and Natural Sciences, University of Bergen, 5020 Bergen, Norway.

Contents of this file

Additional Supporting Information (Files uploaded separately)

QTQt model files

Introduction

The enclosed supplementary information provides full details on the analytical methods used as well as graphical representations of AFT single grain ages and track length distributions. Also included are additional inverse thermal history models and the original QTQt data files (uploaded separately) that can be immediately used by other users to replicate the thermal history inversion.

Text S1

Apatite fission track ages – External Detector Method

During the spontaneous fission of ^{238}U in apatite, damage to the crystal lattice occurs creating a spontaneous fission track. These spontaneous fission tracks accumulate in the apatite crystal over time and are readily quantified by counting tracks which intersect a polished surface under an optical microscope within a defined area. To estimate the abundance of parent isotopes (i.e. ^{238}U), fission of ^{235}U is induced and a mica external detector is used to record induced fission tracks. As the neutron flux during irradiation is monitored using the standard glasses within the sample stack, the number of induced tracks in the mica can be counted and is representative of the ^{235}U content of the grain. ^{238}U can then be estimated as the ratio of $^{235}U/^{238}U$ is constant in nature (1/137.88). Using the relative track densities in the AFT age can be measured using the following equation:

$$t = \frac{1}{\lambda_d} \mathrm{Ln}\left(\lambda_d \frac{\rho_s}{\rho_i} \rho_d \zeta g + 1\right)$$

Where t = age; ρ_s = spontaneous track density; ρ_i = induced track density; ρ_d= track density in a dosimeter (a standard glass of known uranium concentration); g = geometry factor which defines the relationship between spontaneous tracks that intersect the polished surface and induced tracks; and ζ = a constant of proportionality which includes the fission decay constant. The value of ζ is calculated by each fission track analyst and provides a means of standardising the counting process. The external detector method (EDM) (Hurford and Green, 1982) permits individual grains to be dated, even in the presence of heterogeneous uranium distribution.

Apatite (U-Th-Sm)/He Analysis

The majority of single grain AHe analyses were performed by M. Wildman at the Scottish Universities Environmental Research Centre (SUERC) with a smaller proportion of analysis at University College London (UCL). Similar ages and dispersion of ages of the Durango apatite standard were obtained from both facilities. AHe analysis for samples SR-17 and V-10 were analysed by V. Mackintosh at the University of Melbourne. Analytical details for these analyses can be found in Gleadow et al., 2015.

Helium Extraction

A manual He extraction line was used at SUERC after Foeken et al. (2006). He extraction at UCL was performed using a Patterson Instruments automated He extraction system. Single crystal aliquots were packed in Pt foil capsules and placed in 2 mm deep holes in a Cu planchet. The Cu planchet sat within a stainless steel chamber, which was closed, securely tightened and moved into position under the laser. The chamber and flexible steel tube connecting it to the extraction line were then pumped clean using a combination of turbo molecular and ion pumps, which clean the line of atmospheric H and He and generates a vacuum of pressure $<10^{-9}$ torr. Heating tape was placed around both the chamber and flexi-tube for at least 24 hours to remove background CH_4 and H_20. Leak tests were routinely carried out during and following the cleaning procedure of the extraction system to ensure there was no leak in the system. Cold blanks were systematically run to ensure that no contamination of the extraction system had taken place. Hot blanks involving the heating of empty Pt capsules were also performed to ensure the capsule itself is not a significant source of He. A diode

laser system (λ = 808 nm) was used to heat samples to c. 800°C. This method heats the crystal indirectly to a temperature that will allow diffusive loss of He but will not melt the crystal itself.

A HidenHAL3F quadrupole mass spectrometer and a Balzers quadrupole mass spectrometer were used for gas measurements at SUERC and UCL, respectively. He concentrations from samples are calculated against a calibration standard of ^{4}He which is obtained by repeat measurements of the ^{4}He standard throughout the analysis, typically with a reproducibility of (1 – 2%).

U, Th and Sm analysis

Following helium extraction, aliquots were spiked with a calibrated solution with a known concentration of ^{235}U, ^{230}Th and ^{149}Sm, which allowed the relative abundances of ^{238}U, ^{232}Th and ^{147}Sm to be determined. HNO_3 was added to the spike solution to completely dissolve the apatite. At SUERC, samples were analysed using an Agilent 7500ce ICP-MS while at UCL, a Agilent 7700x ICP-MS system was used. A blank vial of HNO_3 and vials of a U standard with known U^{238} concentration were added to the ICP-MS run so that sample measurements can be calibrated.

Apatite (U-Th-Sm)/He age calculation

Once the amount of He, U, Th and Sm have been measured, the (U-Th-Sm)/He age can be calculated using the following equation:

$$[He]=8\left(\frac{137.88}{1+137.88}\right)[U]\left(e^{\lambda_{238}t}-1\right)+7\left(\frac{1}{(1+137.88)}\right)[U]\left(e^{\lambda_{235}t}-1\right)+6[Th]\left(e^{\lambda_{232}t}-1\right)+0.1499[Sm]\left(e^{\lambda_{147}t}-1\right)$$

Where [U], [Th] and [Sm] are the concentrations of uranium, thorium and samarium respectively; λ is the relevant U and Th decay constant (λ_{238} = $1.55\times10^{-10}.yr^{-1}$; λ_{235} = $9.85\times10^{-10}.yr^{-1}$; λ_{232} = $4.95\times10^{-11}.yr^{-1}$, λ_{147} = $6.54\times10^{-12}.yr^{-1}$ and t is the age. The value of 137.88 is determined from the ratio of U^{238} to U^{235}, assumed to be constant in nature.

Figure S2

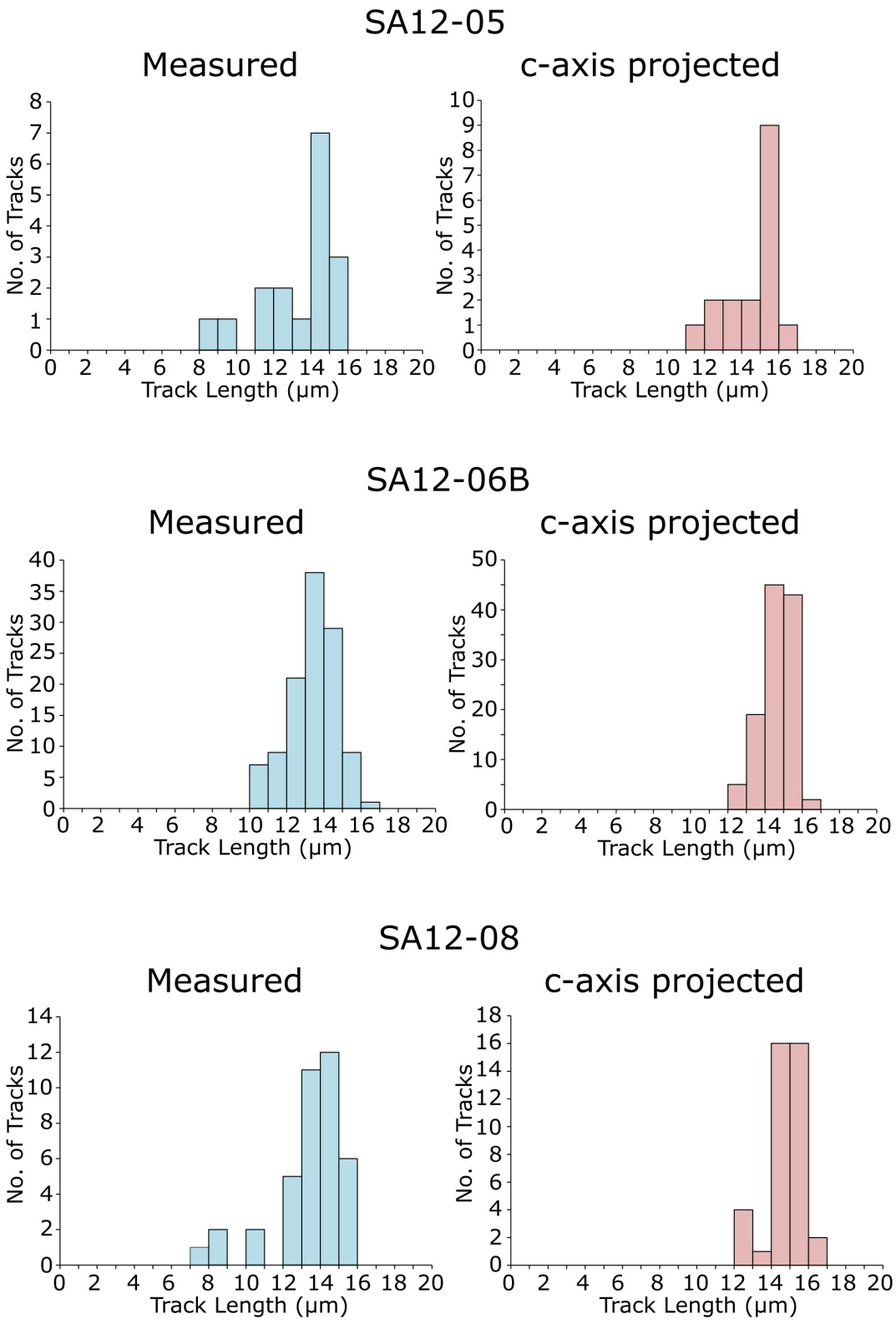
SA12-05
Measured
c-axis projected
No. of Tracks
Track Length (μm)
SA12-06B
Measured
c-axis projected
No. of Tracks
Track Length (μm)
SA12-08
Measured
c-axis projected
No. of Tracks
Track Length (μm)

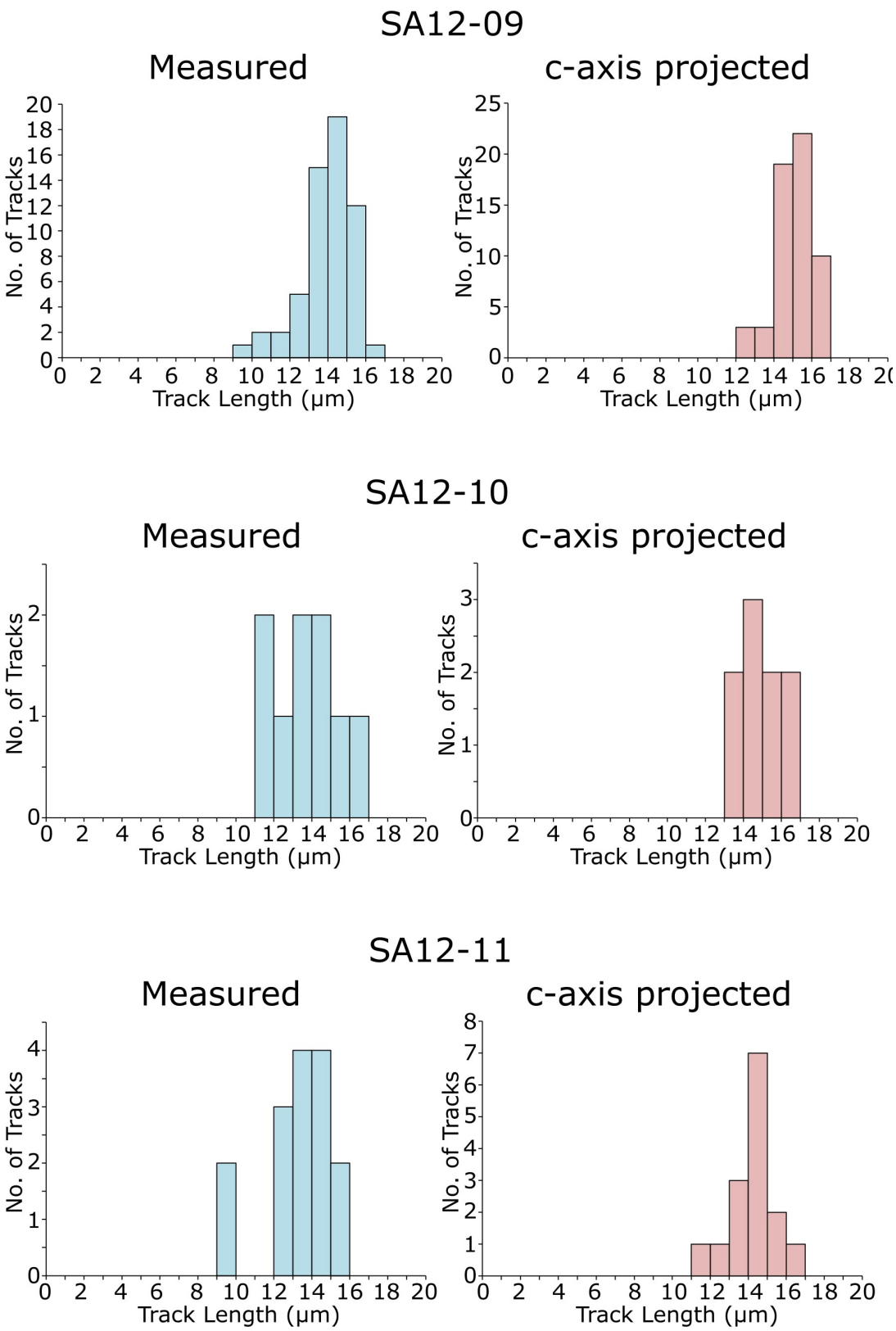
SA12-09
Measured
c-axis projected
No. of Tracks
Track Length (μm)
SA12-10
Measured
c-axis projected
No. of Tracks
Track Length (μm)
SA12-11
Measured
c-axis projected
No. of Tracks
Track Length (μm)

SA12-12

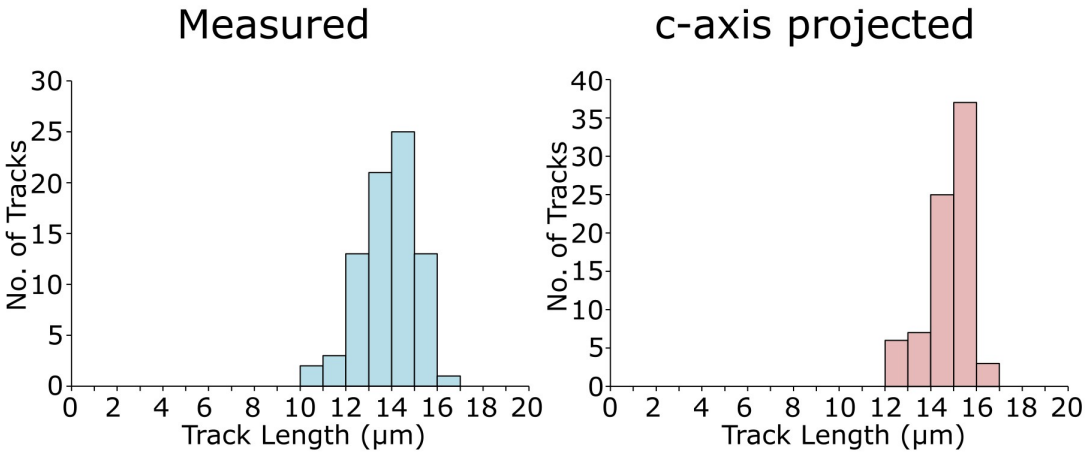

SA12-13A

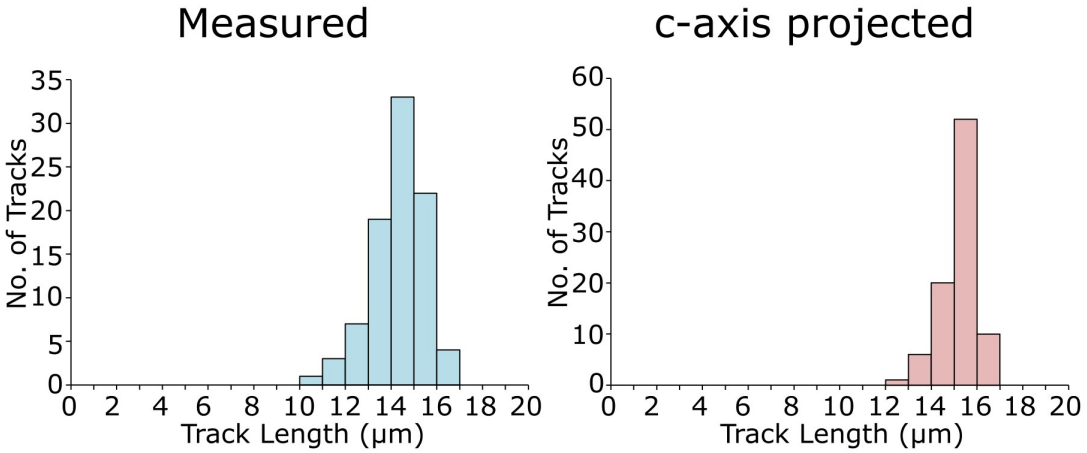

SA12-14

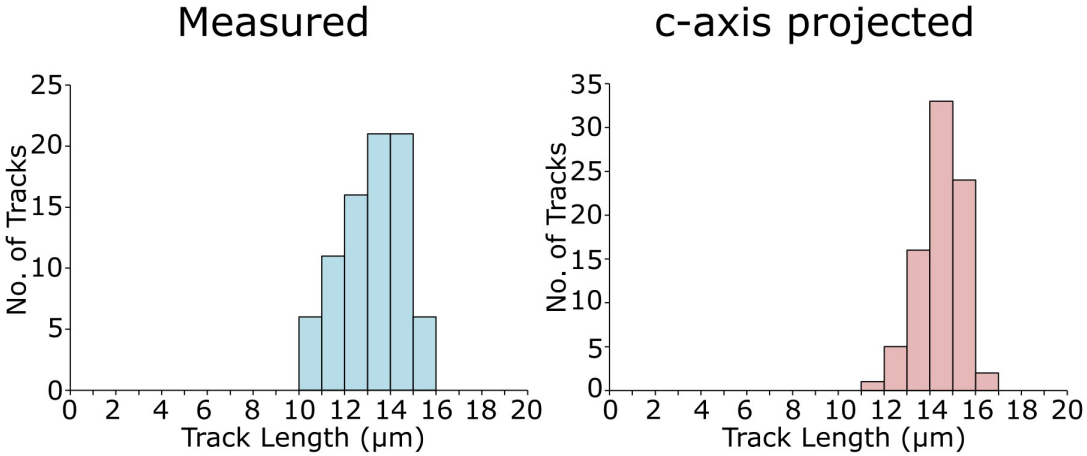

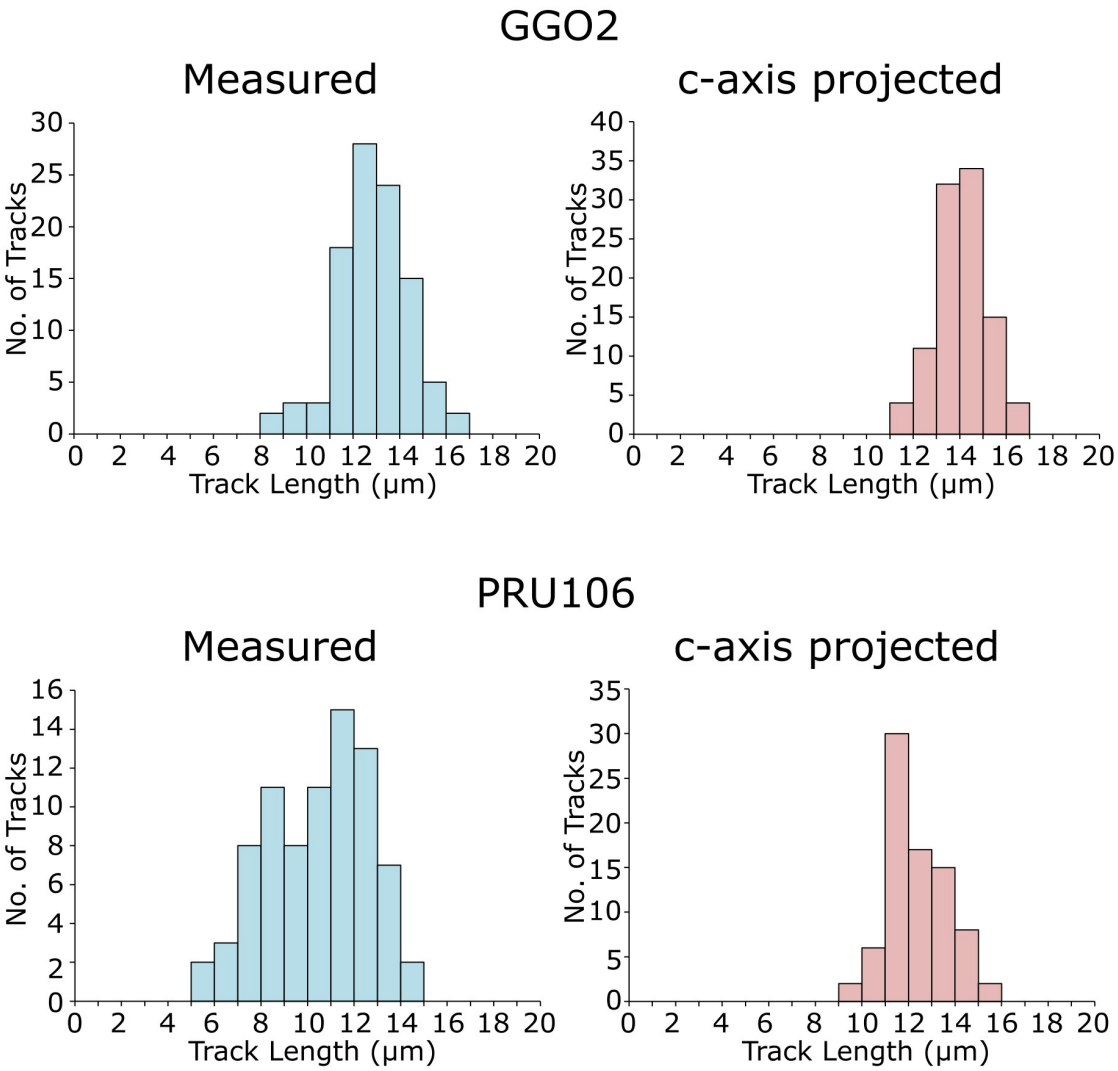
GGO2
Measured
c-axis projected
No. of Tracks
Track Length (μm)
PRU106
Measured
c-axis projected
No. of Tracks
Track Length (μm)

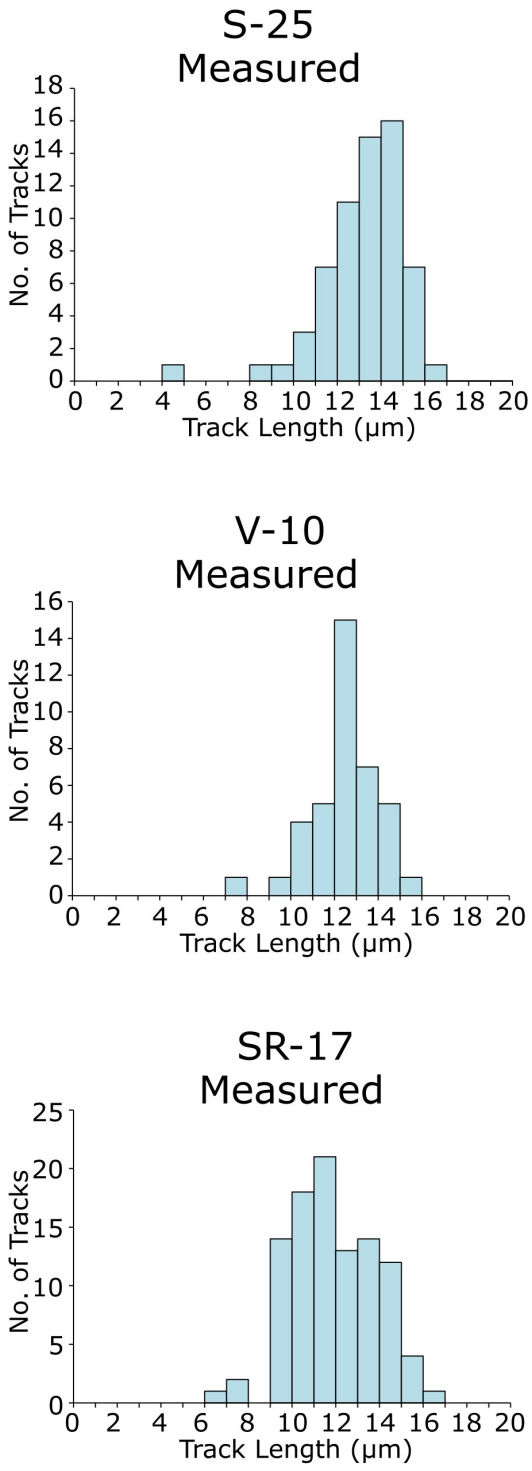

Figure S2: Fission track length distributions for all analysed samples. Both raw track length distributions and track length distributions corrected for orientation to c-axis are shown except for S-25, V-10, SR-17, as these data were collected prior to routine measurement of the angle between measured track and c-axis.

Figure S3

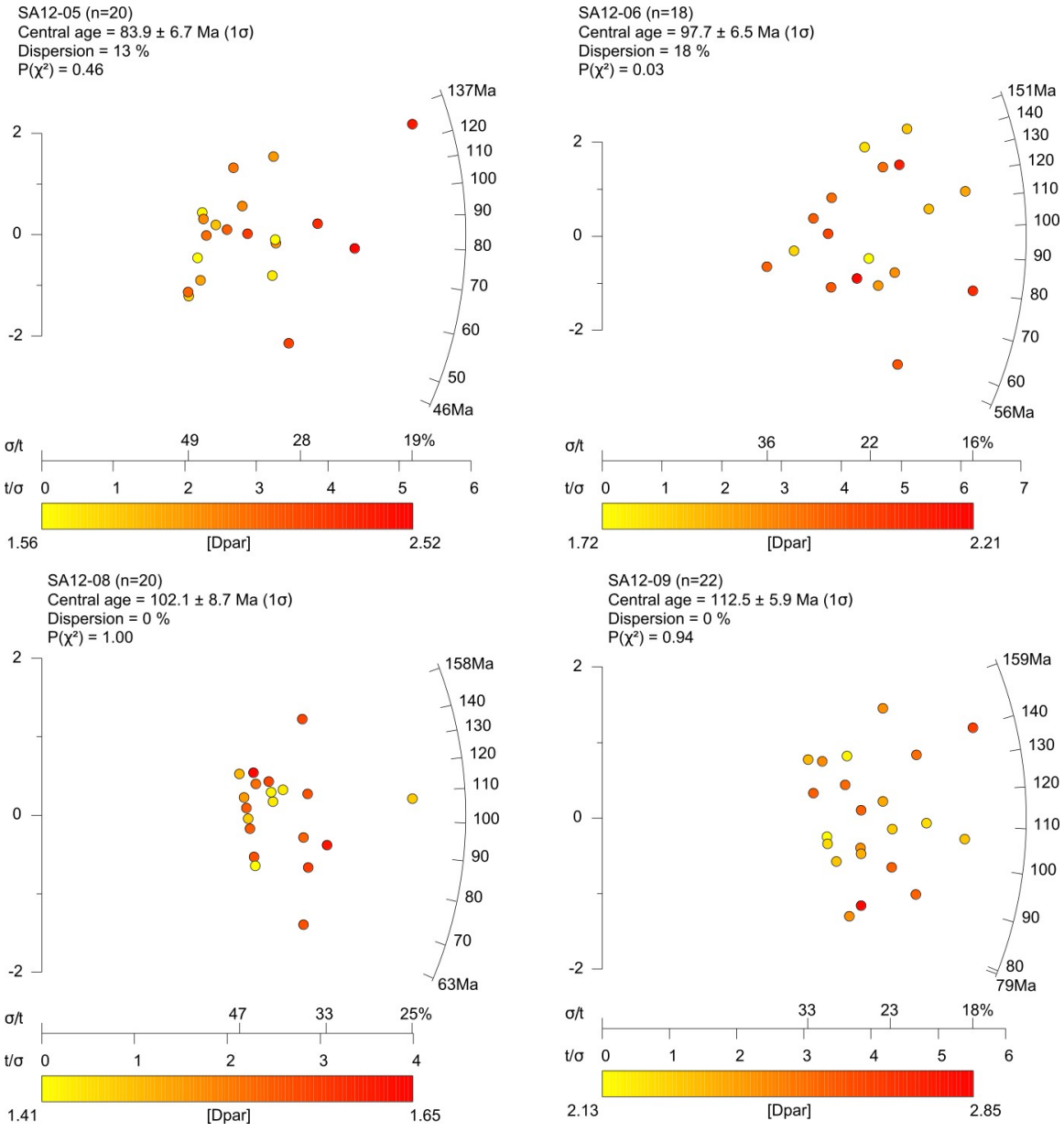
SA12-05 (n=20)
Central age = 83.9 ± 6.7 Ma (1σ)
Dispersion = 13 %
P(χ²) = 0.46
137Ma
120
110
100
90
80
70
60
50
46Ma
2
0
-2
σ/t
49
28
19%
t/σ 0 1 2 3 4 5 6
1.56
[Dpar]
2.52
SA12-06 (n=18)
Central age = 97.7 ± 6.5 Ma (1σ)
Dispersion = 18 %
P(χ²) = 0.03
151Ma
140
130
120
110
100
90
80
70
60
56Ma
2
0
-2
σ/t
36
22
16%
t/σ 0 1 2 3 4 5 6 7
1.72
[Dpar]
2.21
SA12-08 (n=20)
Central age = 102.1 ± 8.7 Ma (1σ)
Dispersion = 0 %
P(χ²) = 1.00
158Ma
140
130
120
110
100
90
80
70
63Ma
2
0
-2
σ/t
47
33
25%
t/σ 0 1 2 3 4
1.41
[Dpar]
1.65
SA12-09 (n=22)
Central age = 112.5 ± 5.9 Ma (1σ)
Dispersion = 0 %
P(χ²) = 0.94
159Ma
140
130
120
110
100
90
80
79Ma
2
0
-2
σ/t
33
23
18%
t/σ 0 1 2 3 4 5 6
2.13
[Dpar]
2.85

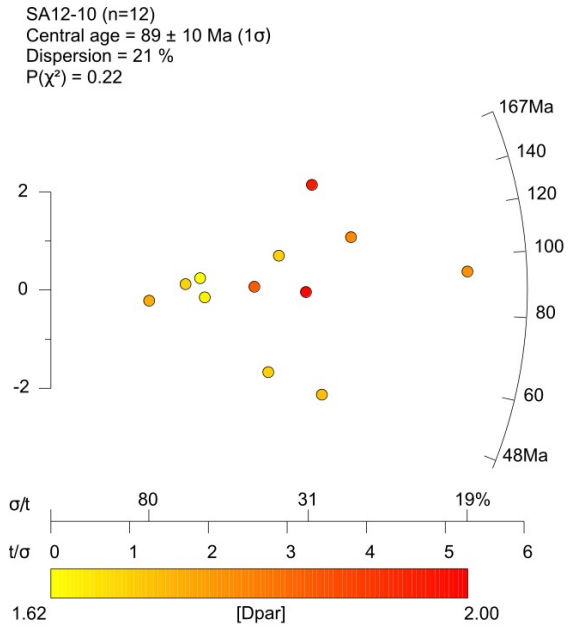
SA12-10 (n=12)
Central age = 89 ± 10 Ma (1σ)
Dispersion = 21 %
P(χ²) = 0.22
167Ma
140
120
100
80
60
48Ma
2
0
-2
σ/t
80
31
19%
t/σ 0 1 2 3 4 5 6
1.62
[Dpar]
2.00

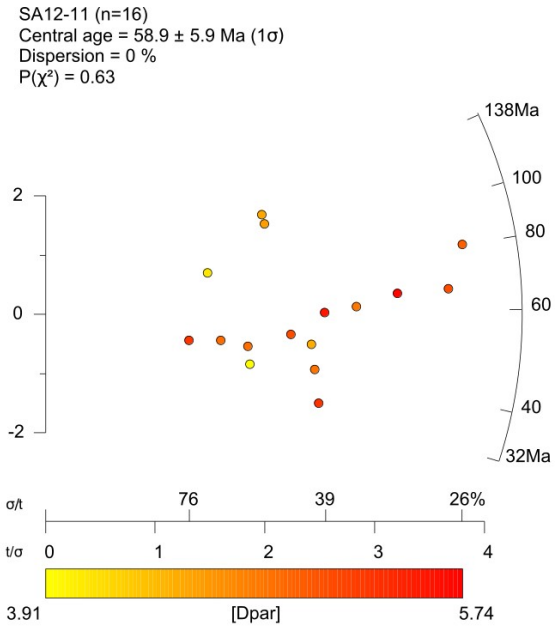
SA12-11 (n=16)
Central age = 58.9 ± 5.9 Ma (1σ)
Dispersion = 0 %
P(χ²) = 0.63
138Ma
100
80
60
40
32Ma
2
0
-2
σ/t
76
39
26%
t/σ 0 1 2 3 4
3.91
[Dpar]
5.74

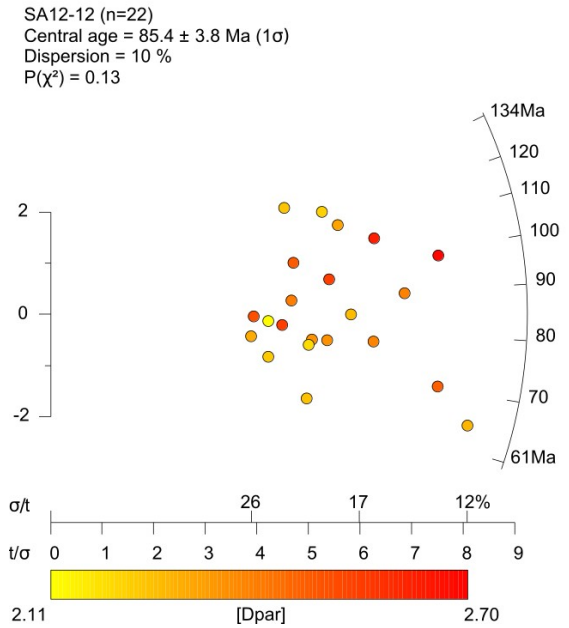
SA12-12 (n=22)
Central age = 85.4 ± 3.8 Ma (1σ)
Dispersion = 10 %
P(χ²) = 0.13
134Ma
120
110
100
90
80
70
61Ma
2
0
-2
σ/t
26
17
12%
t/σ 0 1 2 3 4 5 6 7 8 9
2.11
[Dpar]
2.70

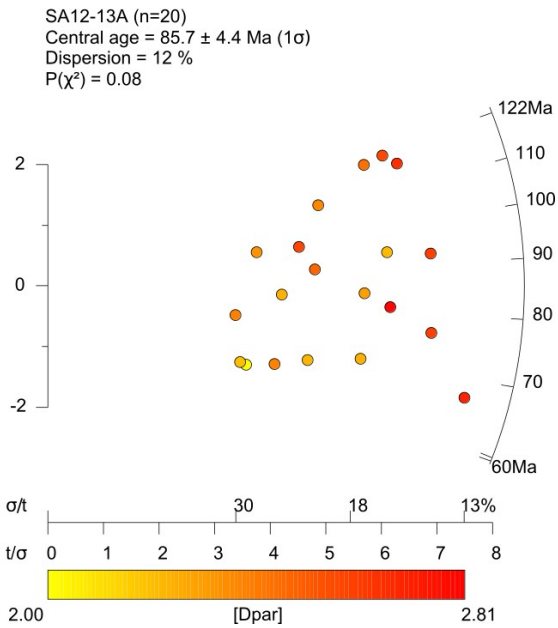
SA12-13A (n=20)
Central age = 85.7 ± 4.4 Ma (1σ)
Dispersion = 12 %
P(χ²) = 0.08
122Ma
110
100
90
80
70
60Ma
2
0
-2
σ/t
30
18
13%
t/σ 0 1 2 3 4 5 6 7 8
2.00
[Dpar]
2.81

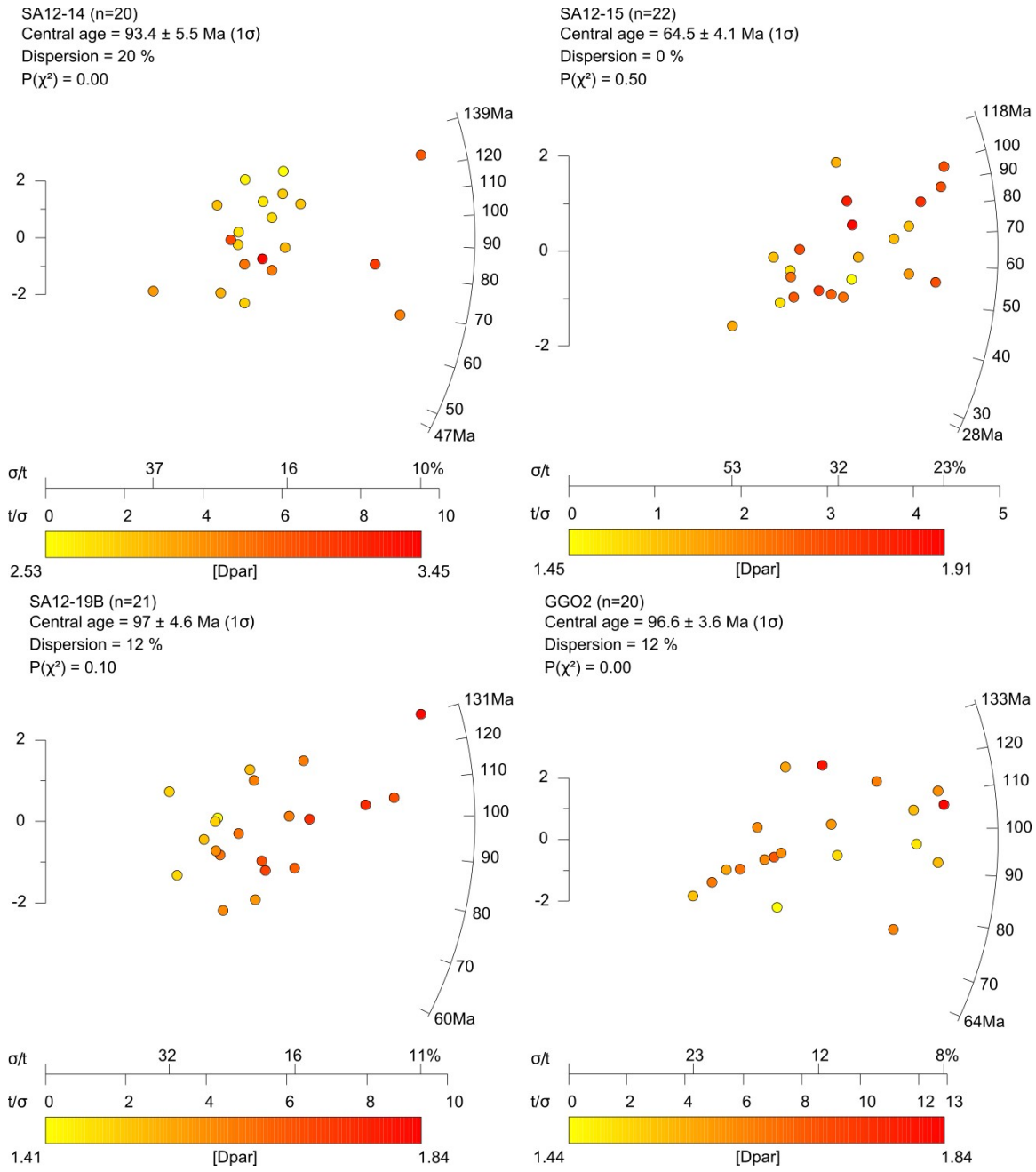
SA12-14 (n=20)
Central age = 93.4 ± 5.5 Ma (1σ)
Dispersion = 20 %
P(χ²) = 0.00
139Ma
120
110
100
90
80
70
60
50
47Ma
2
0
-2
σ/t
37
16
10%
t/σ 0 2 4 6 8 10
2.53
[Dpar]
3.45
SA12-15 (n=22)
Central age = 64.5 ± 4.1 Ma (1σ)
Dispersion = 0 %
P(χ²) = 0.50
118Ma
100
90
80
70
60
50
40
30
28Ma
2
0
-2
σ/t
53
32
23%
t/σ 0 1 2 3 4 5
1.45
[Dpar]
1.91
SA12-19B (n=21)
Central age = 97 ± 4.6 Ma (1σ)
Dispersion = 12 %
P(χ²) = 0.10
131Ma
120
110
100
90
80
70
60Ma
2
0
-2
σ/t
32
16
11%
t/σ 0 2 4 6 8 10
1.41
[Dpar]
1.84
GGO2 (n=20)
Central age = 96.6 ± 3.6 Ma (1σ)
Dispersion = 12 %
P(χ²) = 0.00
133Ma
120
110
100
90
80
70
64Ma
2
0
-2
σ/t
23
12
8%
t/σ 0 2 4 6 8 10 12 13
1.44
[Dpar]
1.84

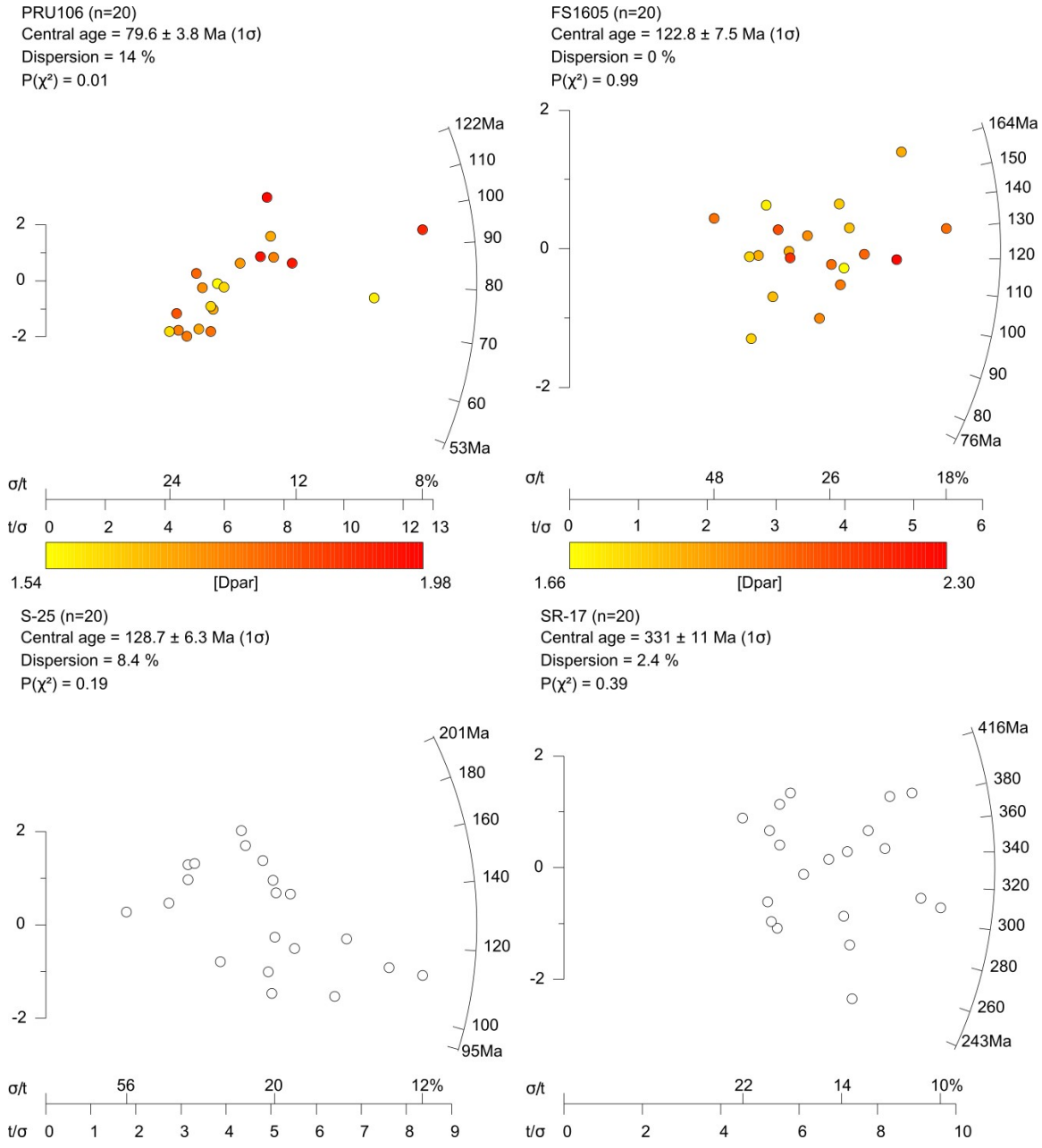
PRU106 (n=20)
Central age = 79.6 ± 3.8 Ma (1σ)
Dispersion = 14 %
P(χ²) = 0.01
122Ma
110
100
90
80
70
60
53Ma
2
0
-2
σ/t
24
12
8%
t/σ 0 2 4 6 8 10 12 13
1.54
[Dpar]
1.98
FS1605 (n=20)
Central age = 122.8 ± 7.5 Ma (1σ)
Dispersion = 0 %
P(χ²) = 0.99
164Ma
150
140
130
120
110
100
90
80
76Ma
2
0
-2
σ/t
48
26
18%
t/σ 0 1 2 3 4 5 6
1.66
[Dpar]
2.30
S-25 (n=20)
Central age = 128.7 ± 6.3 Ma (1σ)
Dispersion = 8.4 %
P(χ²) = 0.19
201Ma
180
160
140
120
100
95Ma
2
0
-2
σ/t
56
20
12%
t/σ 0 1 2 3 4 5 6 7 8 9
SR-17 (n=20)
Central age = 331 ± 11 Ma (1σ)
Dispersion = 2.4 %
P(χ²) = 0.39
416Ma
380
360
340
320
300
280
260
243Ma
2
0
-2
σ/t
22
14
10%
t/σ 0 2 4 6 8 10

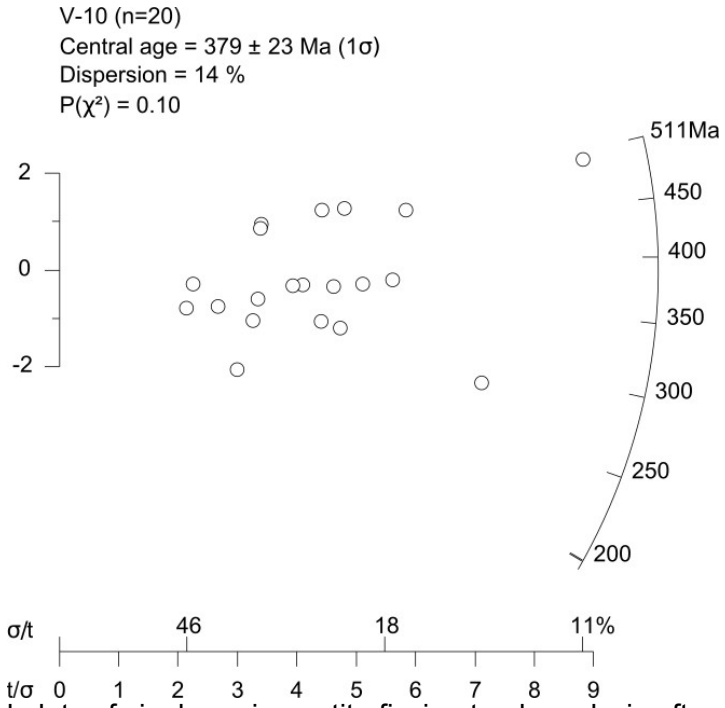

Figure S3: Radial plots of single grain apatite fission track analysis after (Galbraith, 2010). Radial plots were drawn using the Java application RadialPlotter (Vermeesch, 2009).

Plotting single grain AFT ages as a radial plot provides a means to display single grain age dispersion while taking into account the precision of each measurement (Galbraith, 2010). An AFT age (z) with standard error σ is plotted as the point (x, y) where $x = 1/\sigma$ and $y = (z - z_0)/\sigma$ for some z_0 chosen so the average y is near 0. z_0 is the transformation of central AFT age (a logarithmic transformation). Less precise data will plot closer to the origin than more precise data. Each single grain age can be determined using a line which cuts through the origin and the corresponding data point.

A χ^2 test for statistical homogeneity was performed on every sample with the corresponding p-value shown each radial plot. When the p-value is < 0.05, there is the possibility that the sample set contains more than one population. In these cases a mixture model (Galbraith and Green, 1990) was used to investigate whether the single grain age distributions better represent more than one population of ages. Radial lines on the radial plot indicate peak centres and the age of the peaks and proportions of grains belonging to that population are beneath the radial plot. Details of the algorithm used for the mixture modelling can be found in Vermeesch, (2009).

Figure S4 (a)

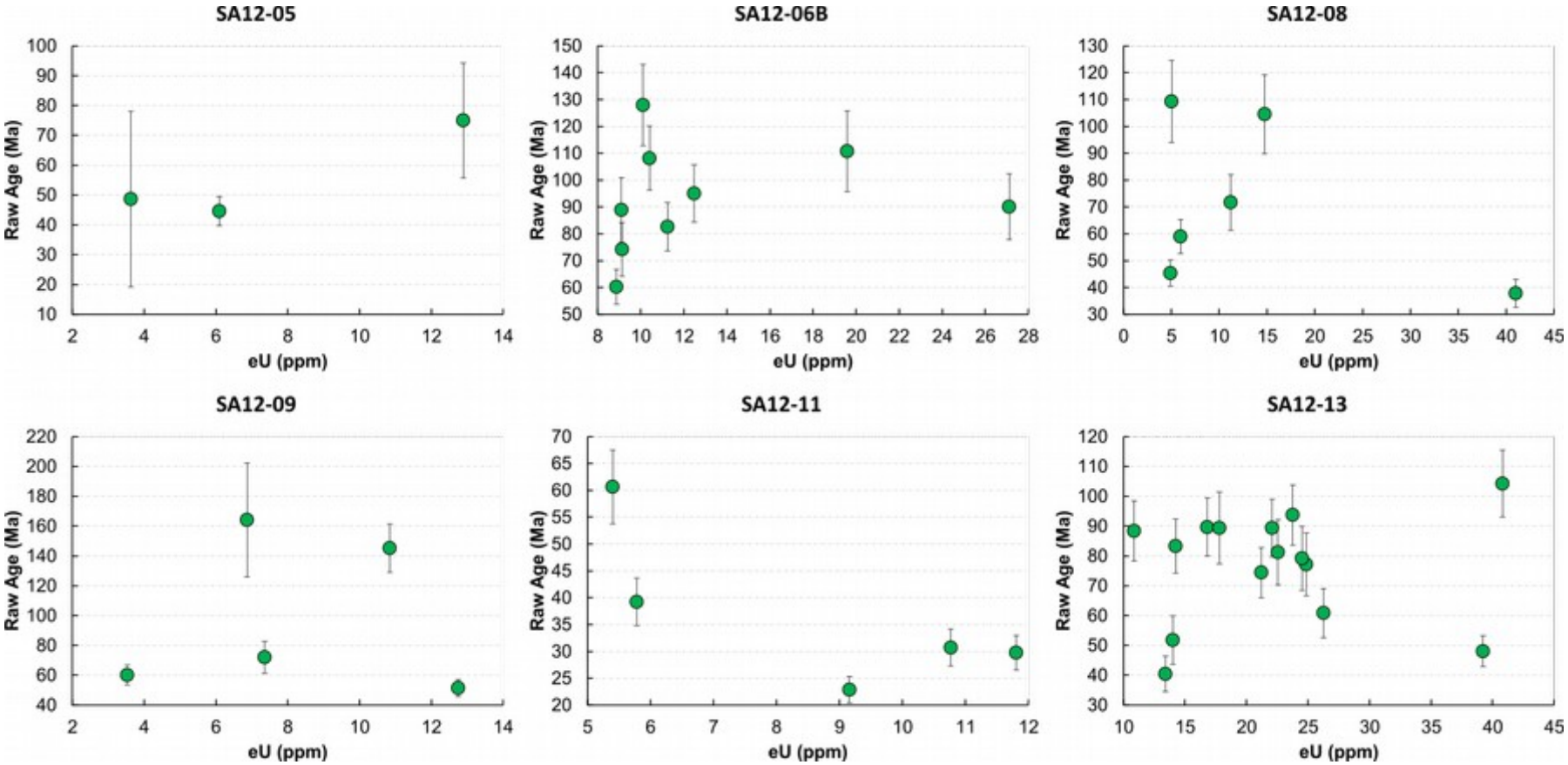
SA12-05
SA12-06B
SA12-08
SA12-09
SA12-11
SA12-13
Raw Age (Ma)
eU (ppm)

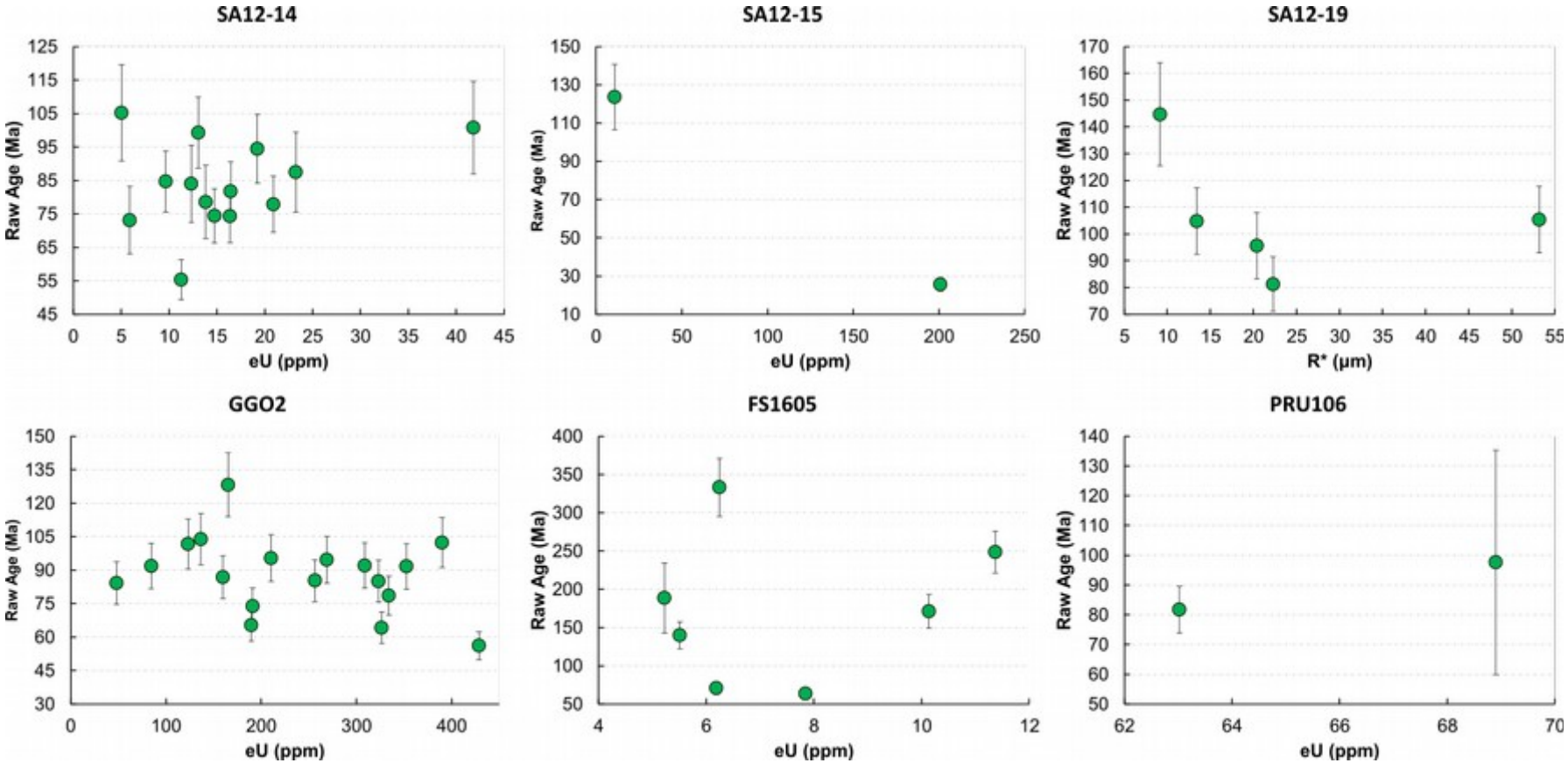
SA12-14
Raw Age (Ma)
eU (ppm)
SA12-15
Raw Age (Ma)
eU (ppm)
SA12-19
Raw Age (Ma)
R* (µm)
GGO2
Raw Age (Ma)
eU (ppm)
FS1605
Raw Age (Ma)
eU (ppm)
PRU106
Raw Age (Ma)
eU (ppm)

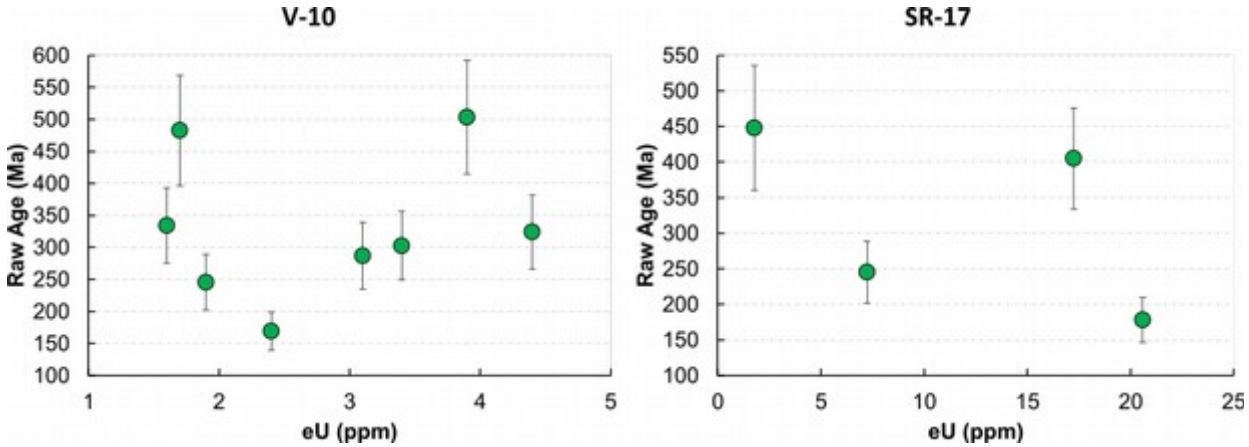
V-10
Raw Age (Ma)
600
550
500
450
400
350
300
250
200
150
100
1
2
3
4
5
eU (ppm)
SR-17
Raw Age (Ma)
550
500
450
400
350
300
250
200
150
100
0
5
10
15
20
25
eU (ppm)

Figure S4 (b)

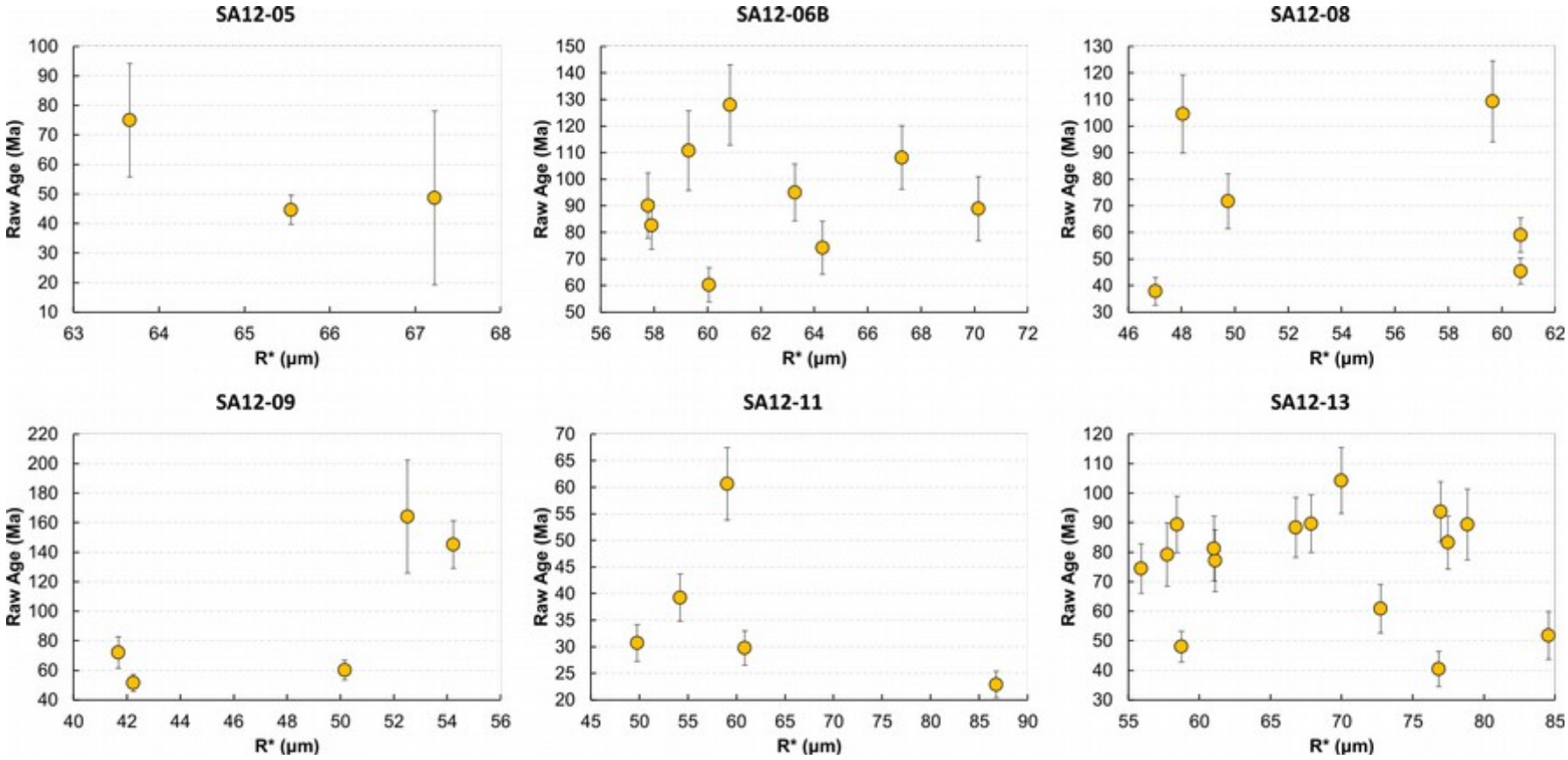

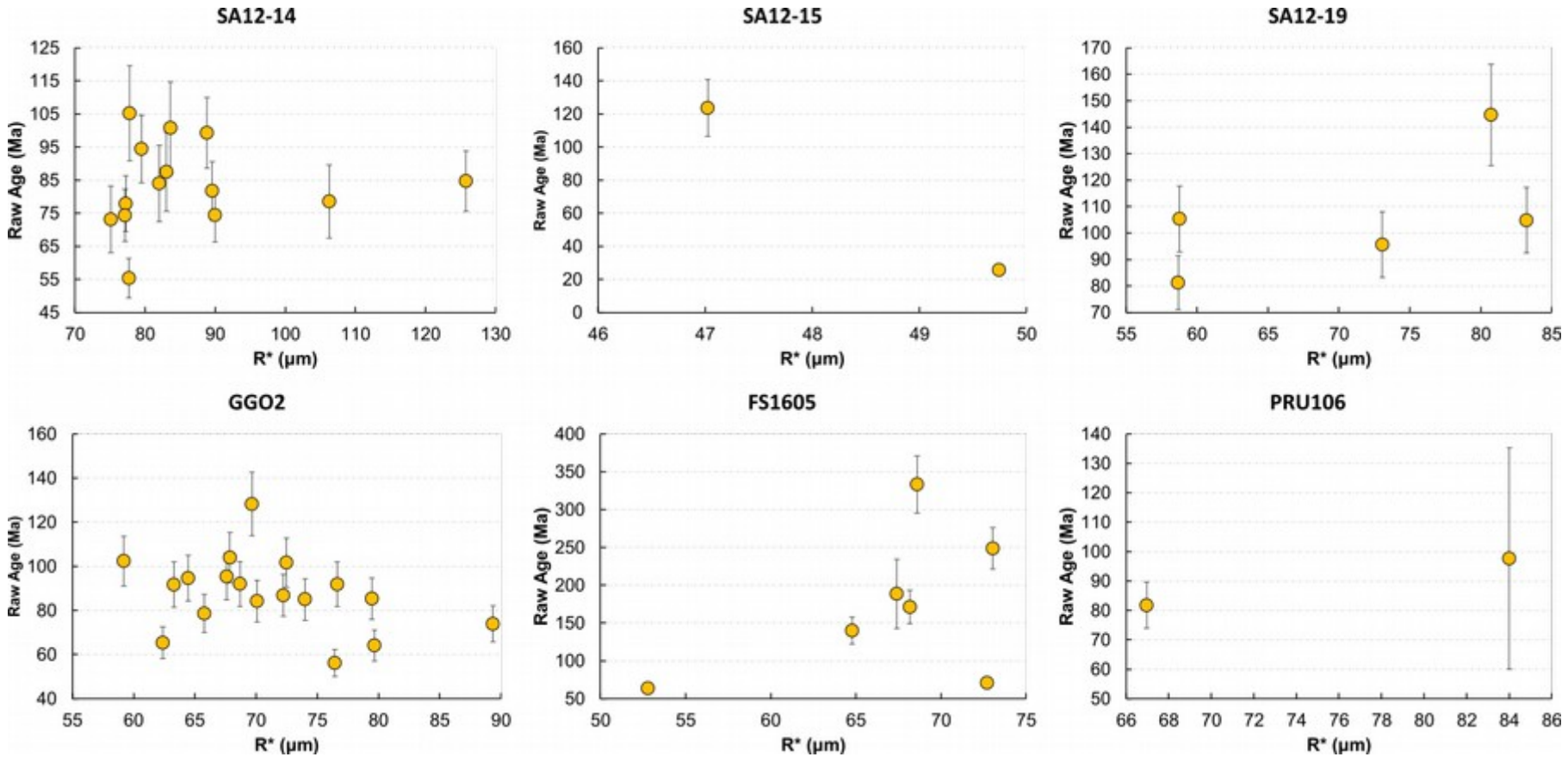
SA12-14
Raw Age (Ma)
R* (µm)
SA12-15
Raw Age (Ma)
R* (µm)
SA12-19
Raw Age (Ma)
R* (µm)
GGO2
Raw Age (Ma)
R* (µm)
FS1605
Raw Age (Ma)
R* (µm)
PRU106
Raw Age (Ma)
R* (µm)

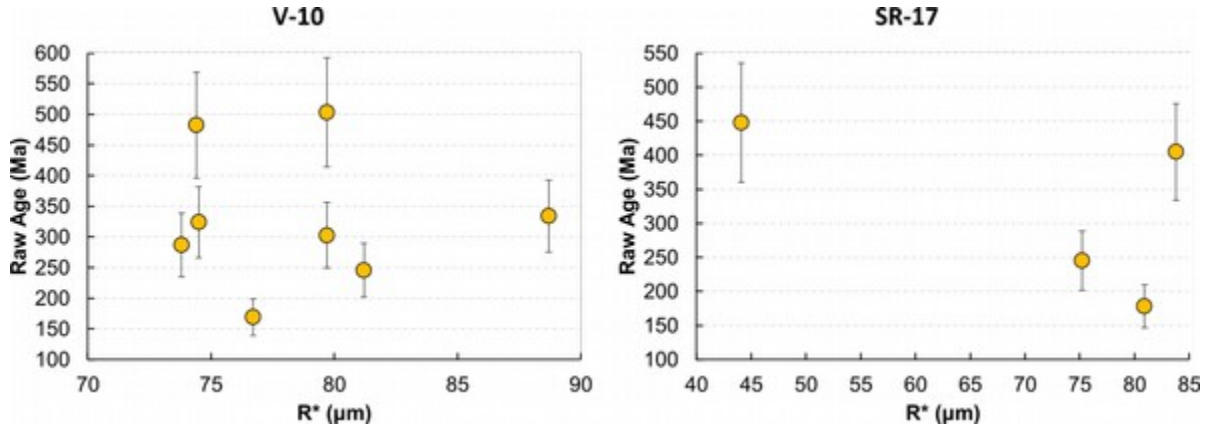

Figure S4: (a) AHe age versus effective Uranium content ([eU] = [U] + 0.235*[Th]); (b) AHe age versus equivalent spherical grain radius.

Figure – S5

SA12-05

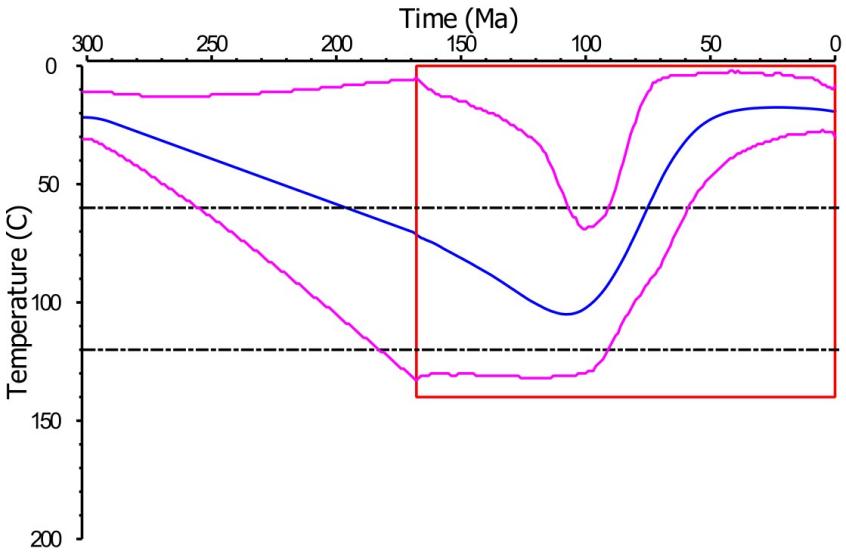

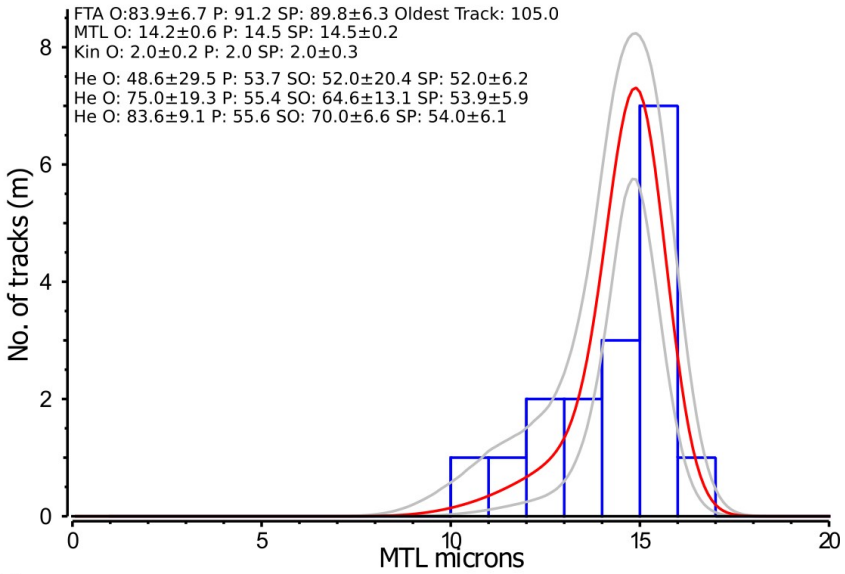

SA12-06

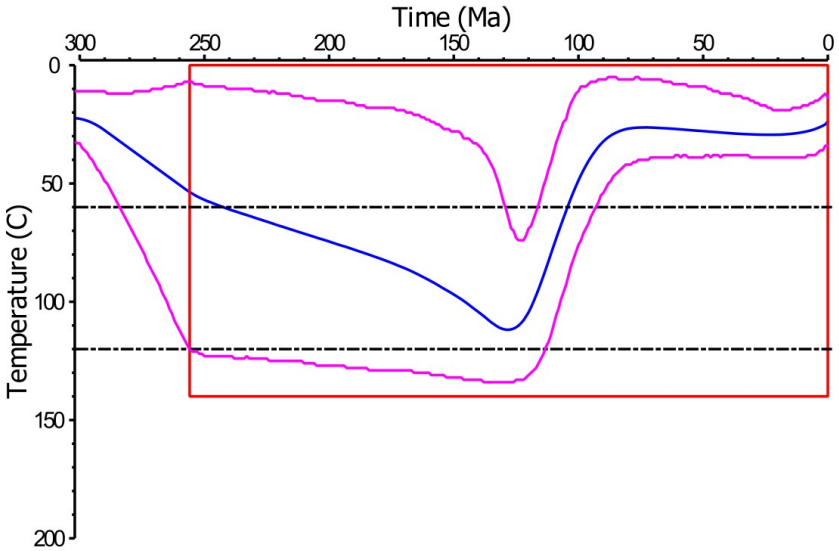

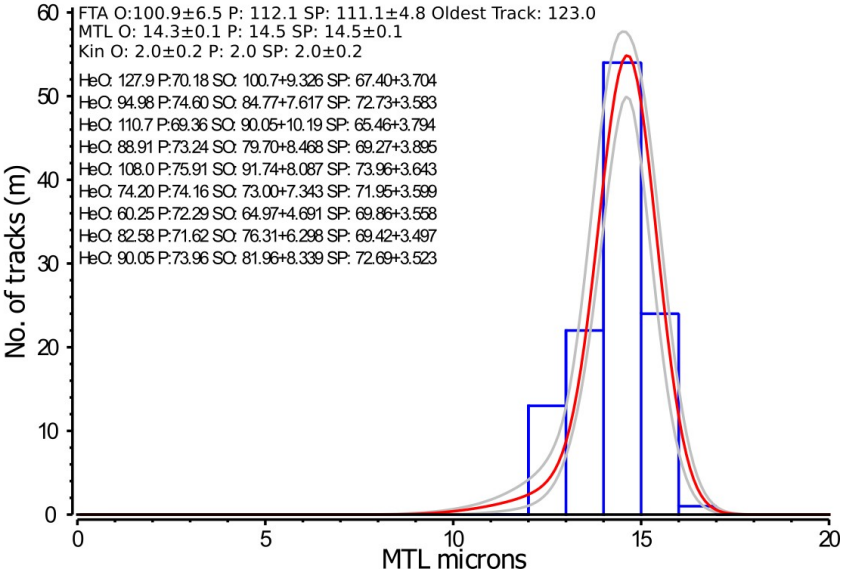

SA12-08

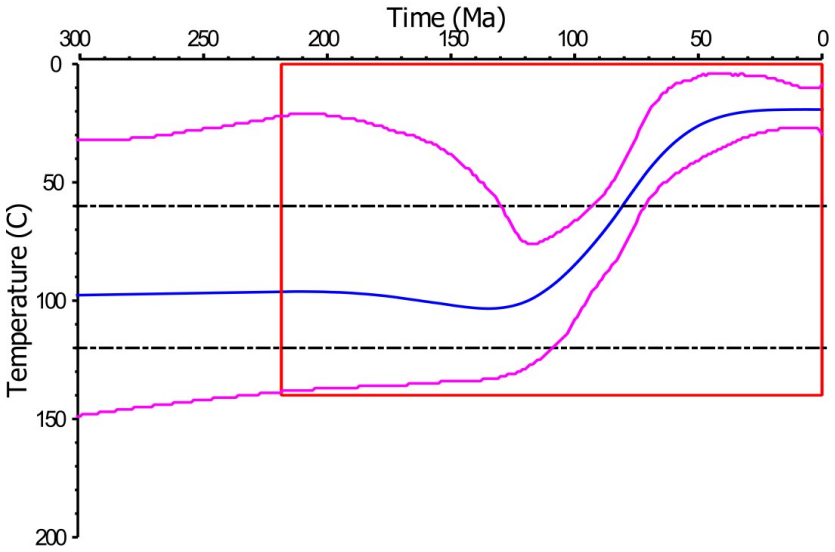

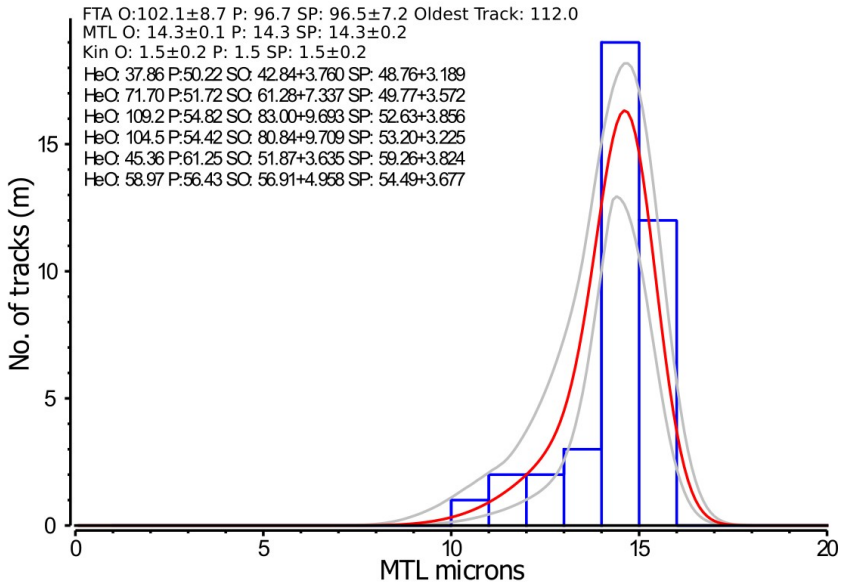

SA12-09

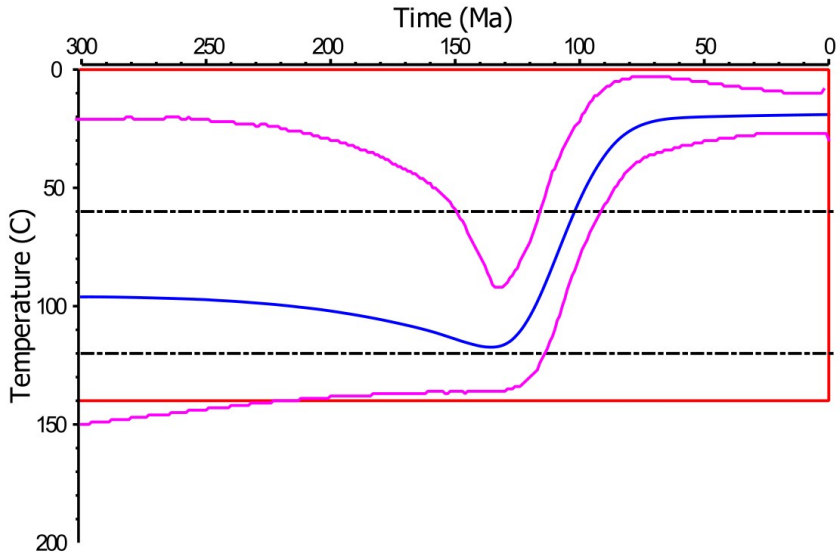

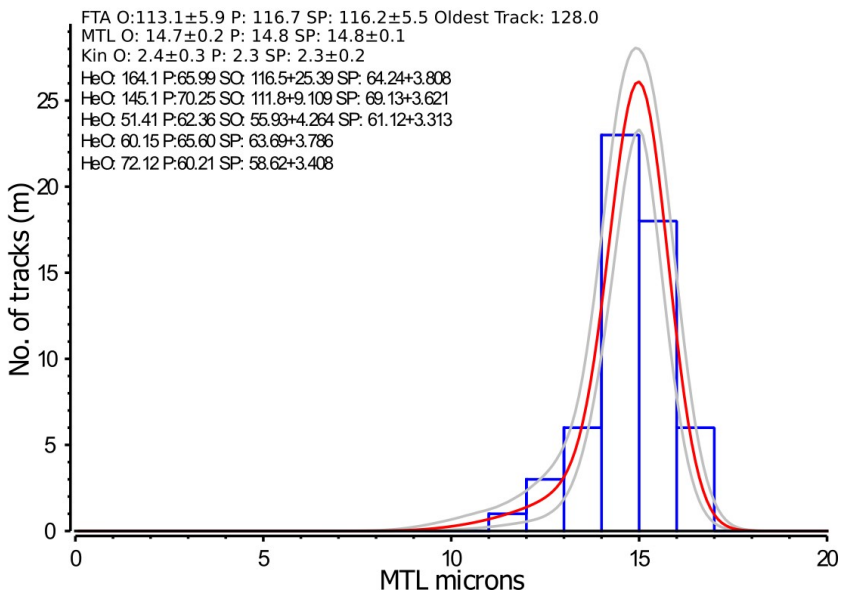

SA12-10

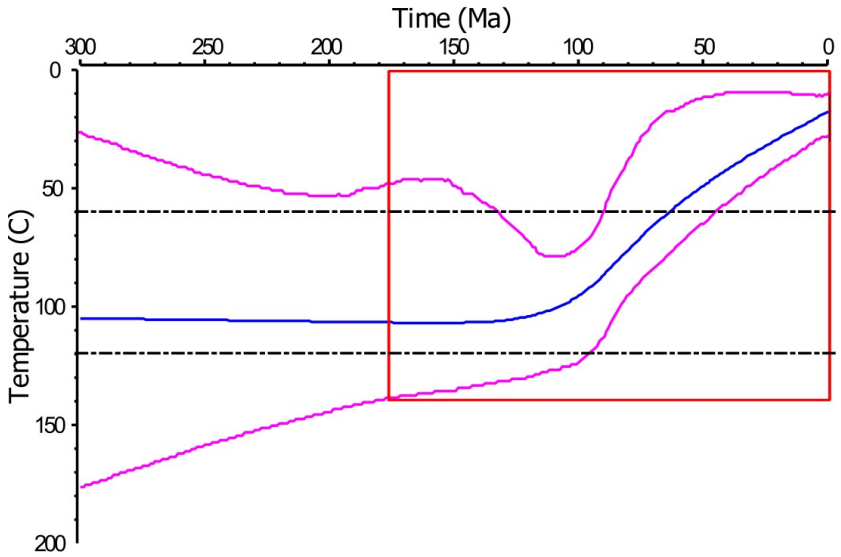

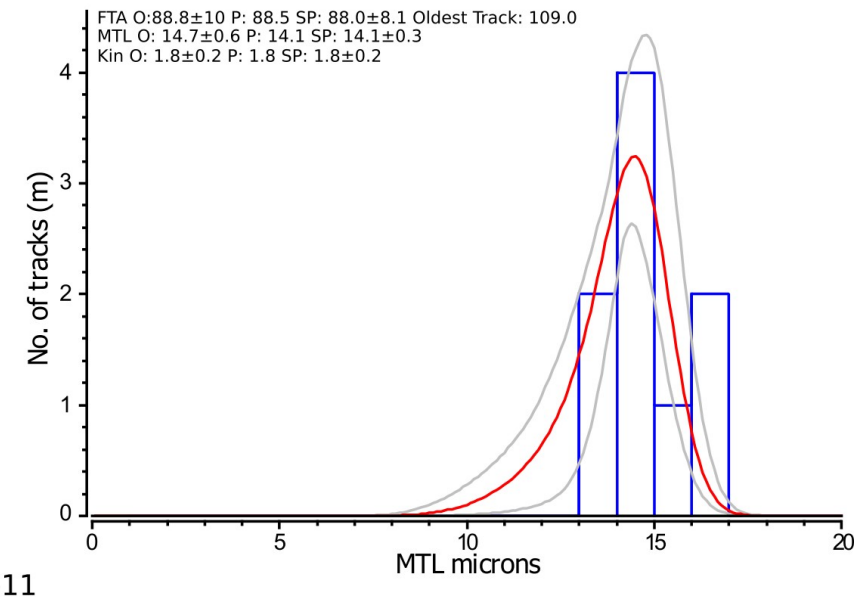

SA12-11

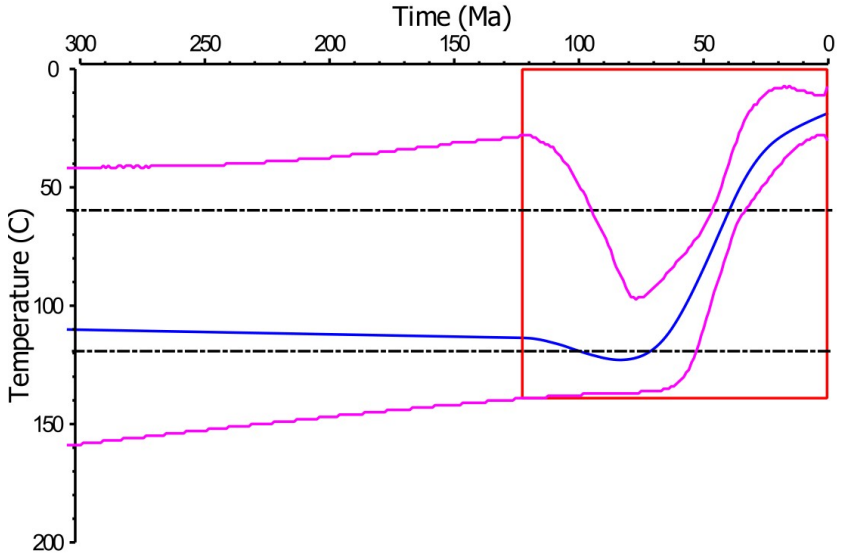

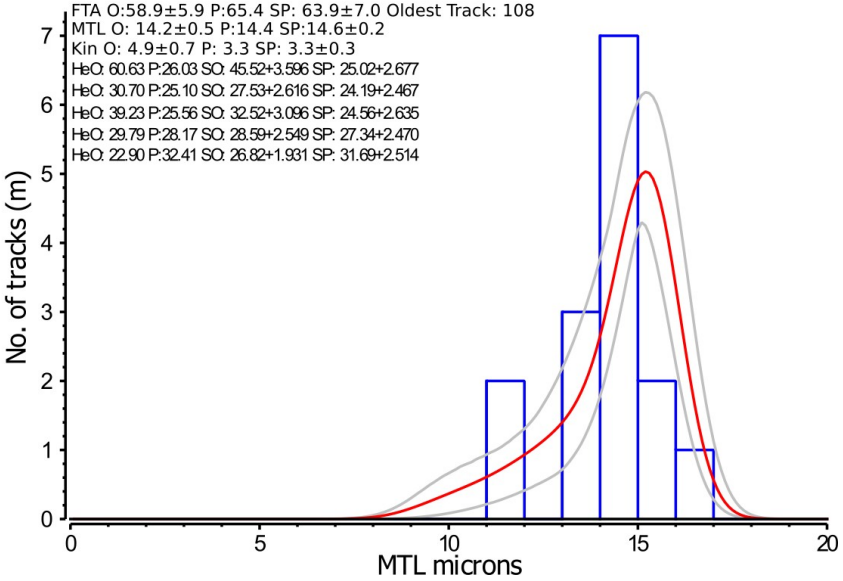

SA12-12

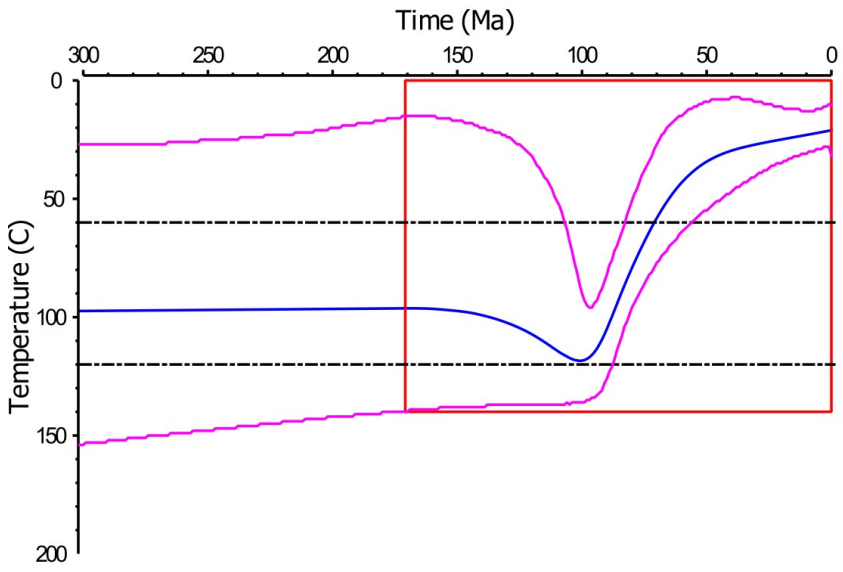

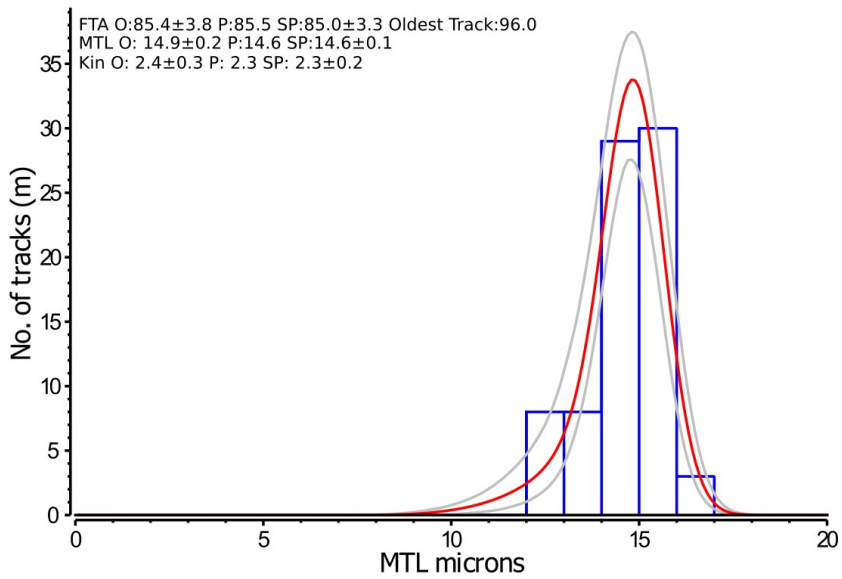

SA12-13

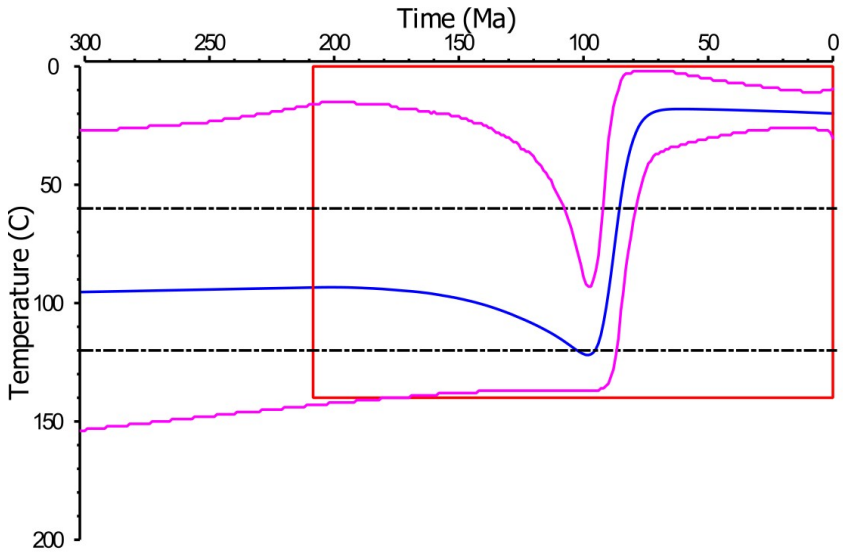

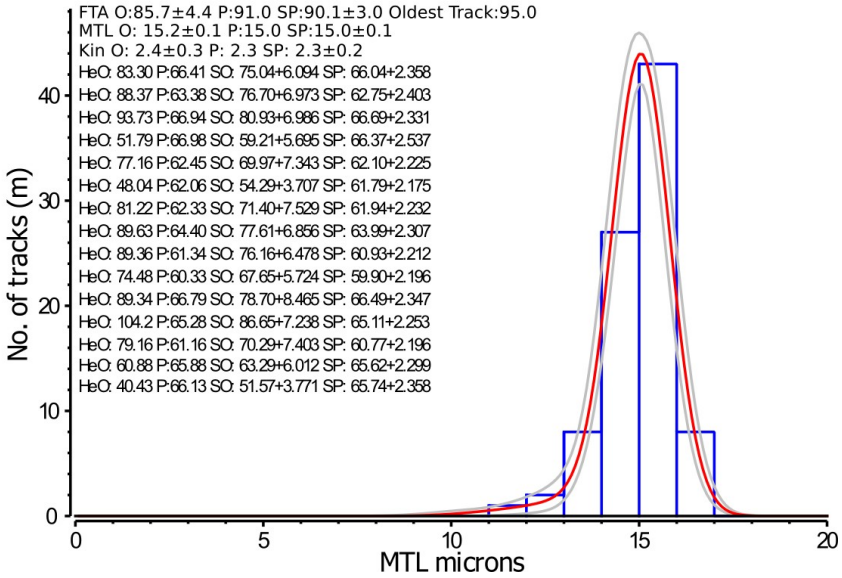

SA12-14

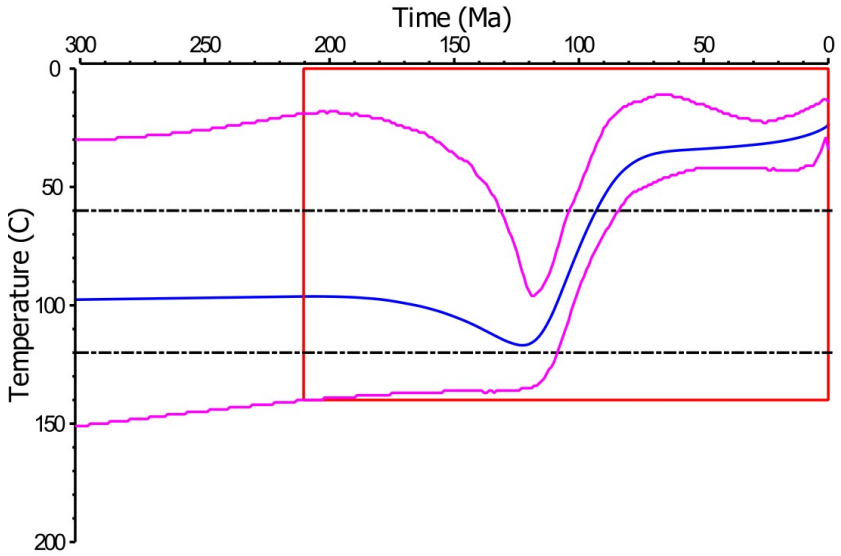

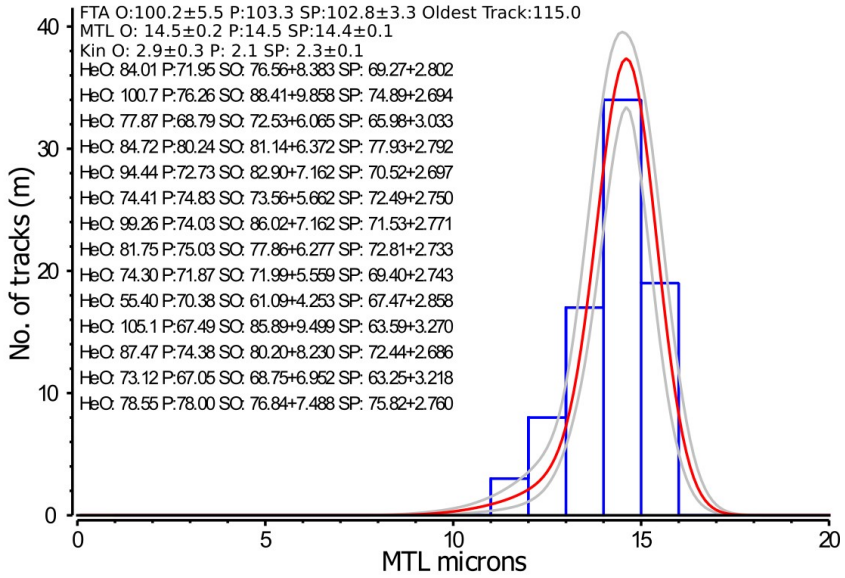

SA12-15

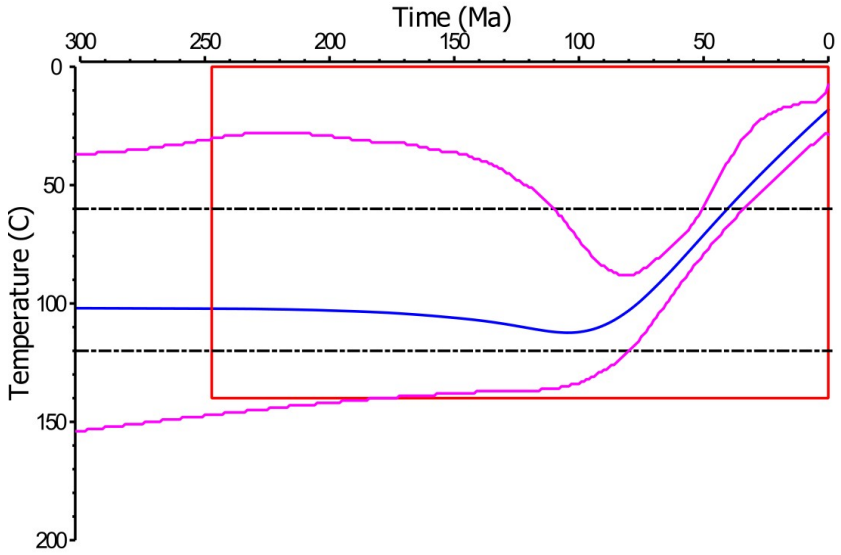

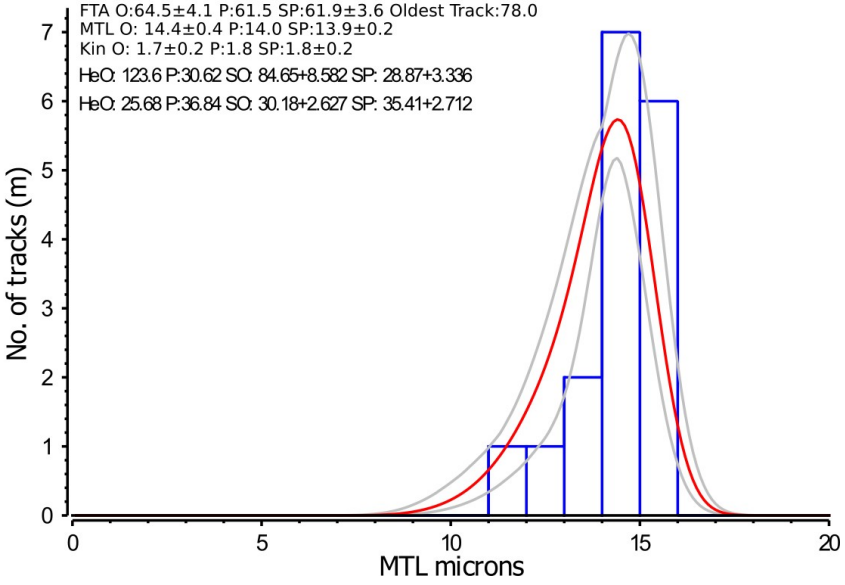

SA12-19B

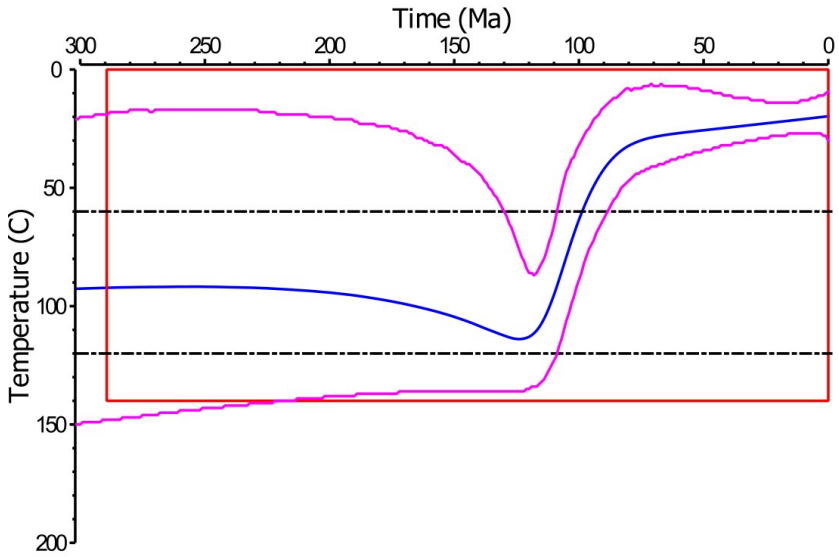

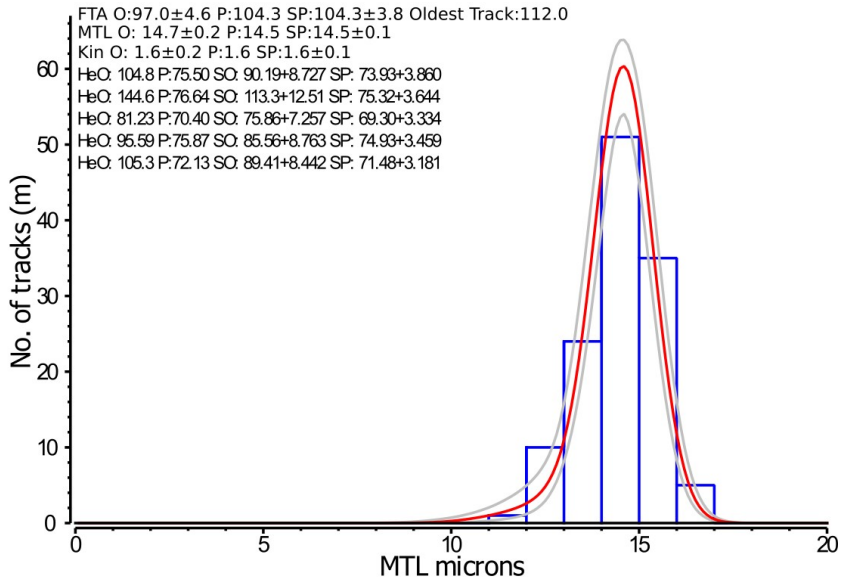

FS1605

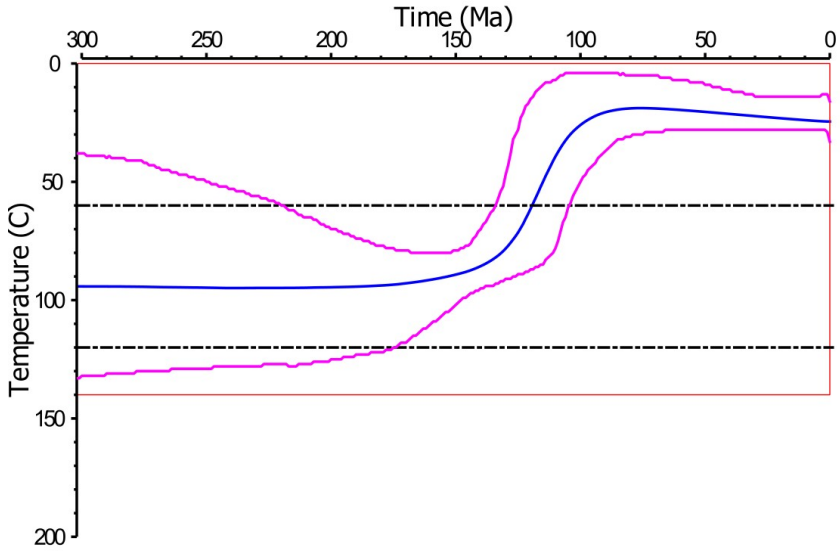

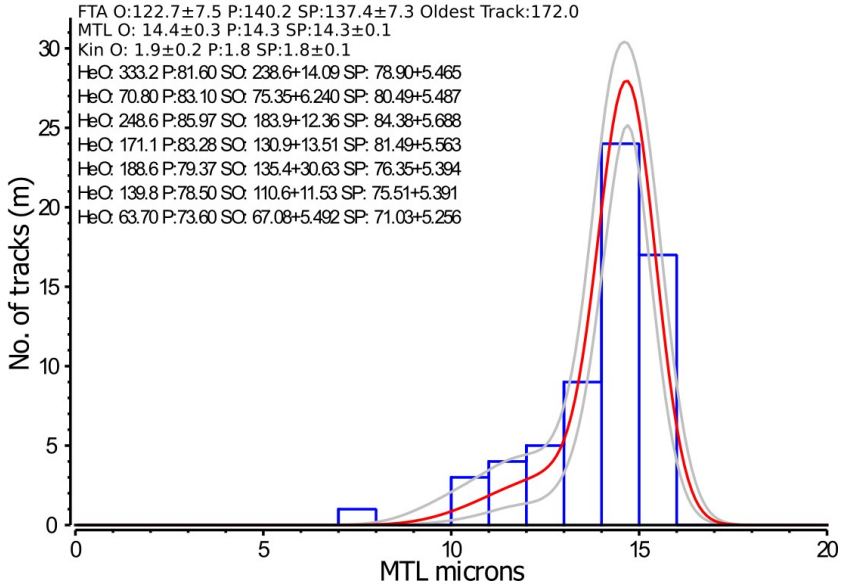

GGO2

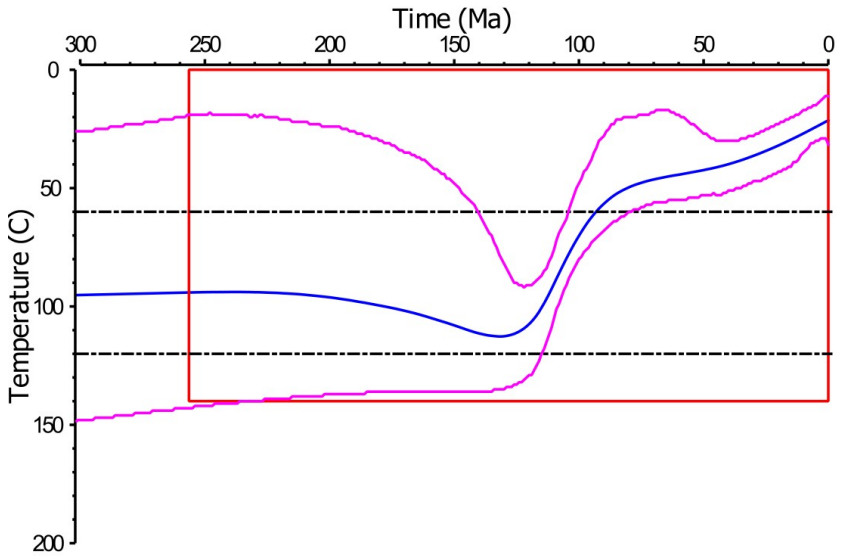
Time (Ma)
300
250
200
150
100
50
0
Temperature (C)
0
50
100
150
200

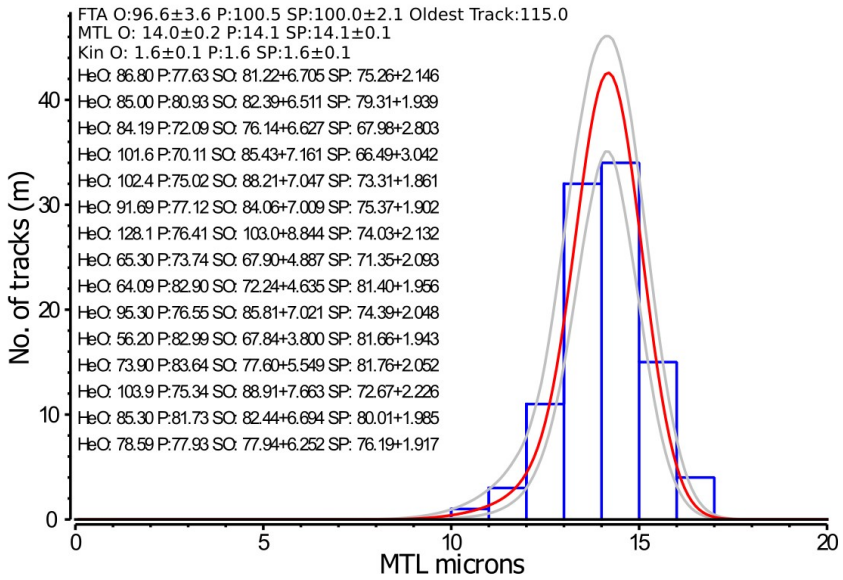
FTA O:96.6±3.6 P:100.5 SP:100.0±2.1 Oldest Track:115.0
MTL O: 14.0±0.2 P:14.1 SP:14.1±0.1
Kin O: 1.6±0.1 P:1.6 SP:1.6±0.1
HeO: 86.80 P:77.63 SO: 81.22+6.705 SP: 75.26+2.146
HeO: 85.00 P:80.93 SO: 82.39+6.511 SP: 79.31+1.939
HeO: 84.19 P:72.09 SO: 76.14+6.627 SP: 67.98+2.803
HeO: 101.6 P:70.11 SO: 85.43+7.161 SP: 66.49+3.042
HeO: 102.4 P:75.02 SO: 88.21+7.047 SP: 73.31+1.861
HeO: 91.69 P:77.12 SO: 84.06+7.009 SP: 75.37+1.902
HeO: 128.1 P:76.41 SO: 103.0+8.844 SP: 74.03+2.132
HeO: 65.30 P:73.74 SO: 67.90+4.887 SP: 71.35+2.093
HeO: 64.09 P:82.90 SO: 72.24+4.635 SP: 81.40+1.956
HeO: 95.30 P:76.55 SO: 85.81+7.021 SP: 74.39+2.048
HeO: 56.20 P:82.99 SO: 67.84+3.800 SP: 81.66+1.943
HeO: 73.90 P:83.64 SO: 77.60+5.549 SP: 81.76+2.052
HeO: 103.9 P:75.34 SO: 88.91+7.663 SP: 72.67+2.226
HeO: 85.30 P:81.73 SO: 82.44+6.694 SP: 80.01+1.985
HeO: 78.59 P:77.93 SO: 77.94+6.252 SP: 76.19+1.917
No. of tracks (m)
0
10
20
30
40
0
5
10
15
20
MTL microns

PRU106

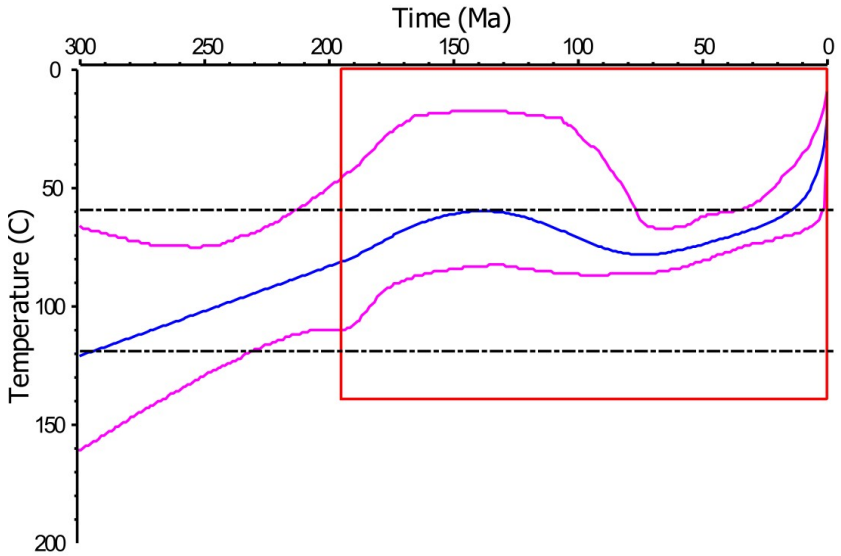
Time (Ma)
300
250
200
150
100
50
0
Temperature (C)
0
50
100
150
200

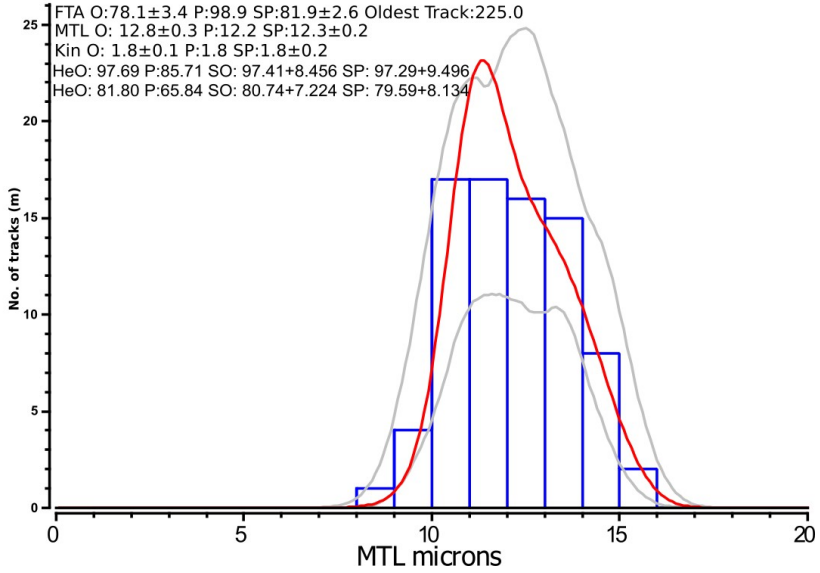
FTA O:78.1±3.4 P:98.9 SP:81.9±2.6 Oldest Track:225.0
MTL O: 12.8±0.3 P:12.2 SP:12.3±0.2
Kin O: 1.8±0.1 P:1.8 SP:1.8±0.2
HeO: 97.69 P:85.71 SO: 97.41+8.456 SP: 97.29+9.496
HeO: 81.80 P:65.84 SO: 80.74+7.224 SP: 79.59+8.134
No. of tracks (m)
0
5
10
15
20
25
0
5
10
15
20
MTL microns

S-25

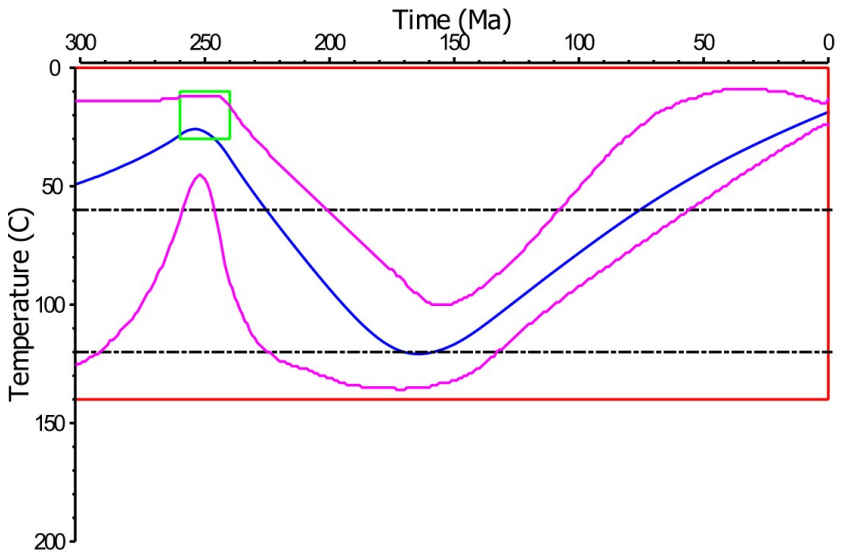
Time (Ma)
300
250
200
150
100
50
0
Temperature (C)
0
50
100
150
200

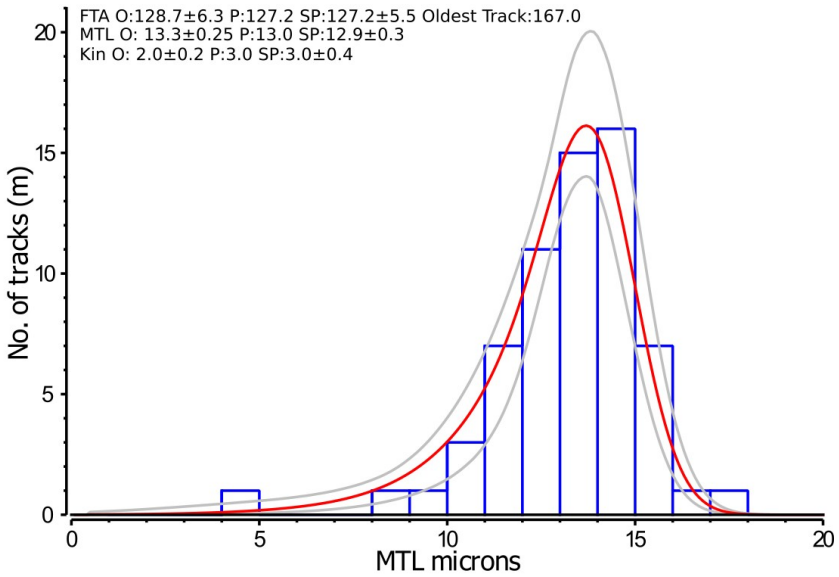
FTA O:128.7±6.3 P:127.2 SP:127.2±5.5 Oldest Track:167.0
MTL O: 13.3±0.25 P:13.0 SP:12.9±0.3
Kin O: 2.0±0.2 P:3.0 SP:3.0±0.4
No. of tracks (m)
0
5
10
15
20
MTL microns

SR-17

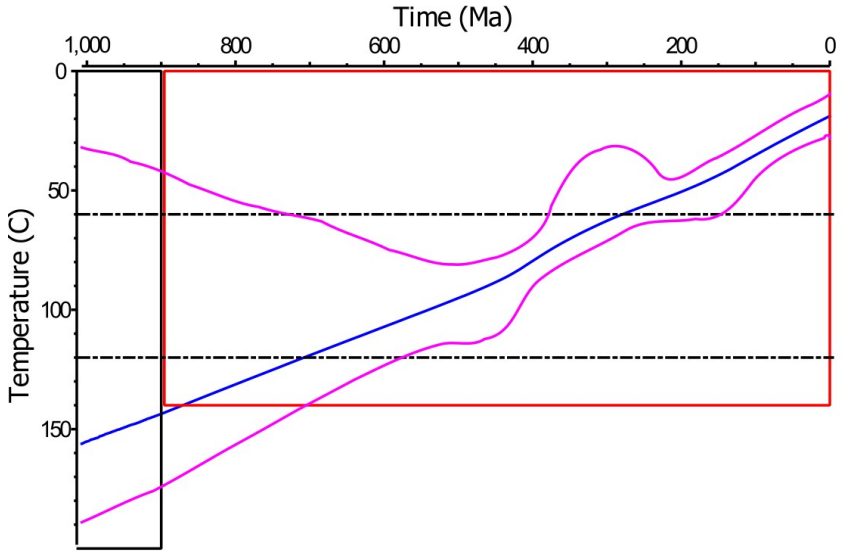
Time (Ma)
1,000
800
600
400
200
0
Temperature (C)
0
50
100
150

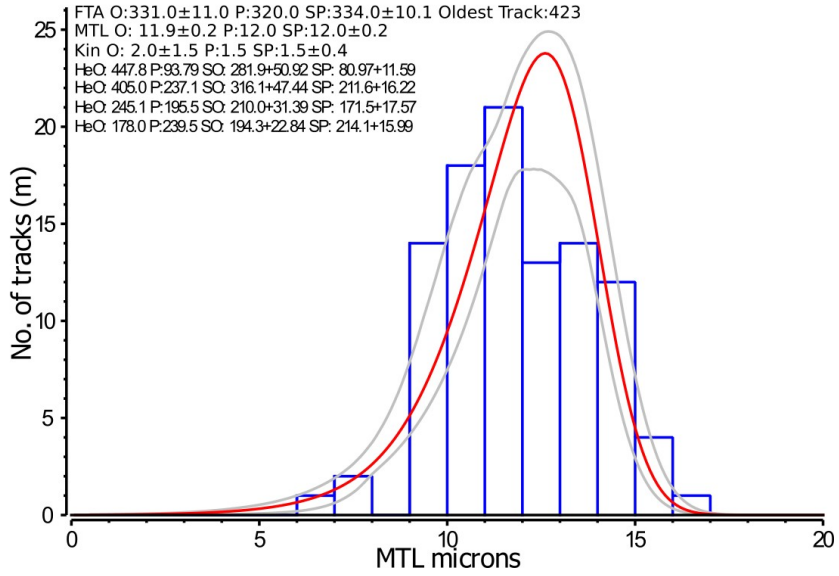
FTA O:331.0±11.0 P:320.0 SP:334.0±10.1 Oldest Track:423
MTL O: 11.9±0.2 P:12.0 SP:12.0±0.2
Kin O: 2.0±1.5 P:1.5 SP:1.5±0.4
HeO: 447.8 P:93.79 SO: 281.9+50.92 SP: 80.97+11.59
HeO: 405.0 P:237.1 SO: 316.1+47.44 SP: 211.6+16.22
HeO: 245.1 P:195.5 SO: 210.0+31.39 SP: 171.5+17.57
HeO: 178.0 P:239.5 SO: 194.3+22.84 SP: 214.1+15.99
No. of tracks (m)
0
5
10
15
20
25
MTL microns

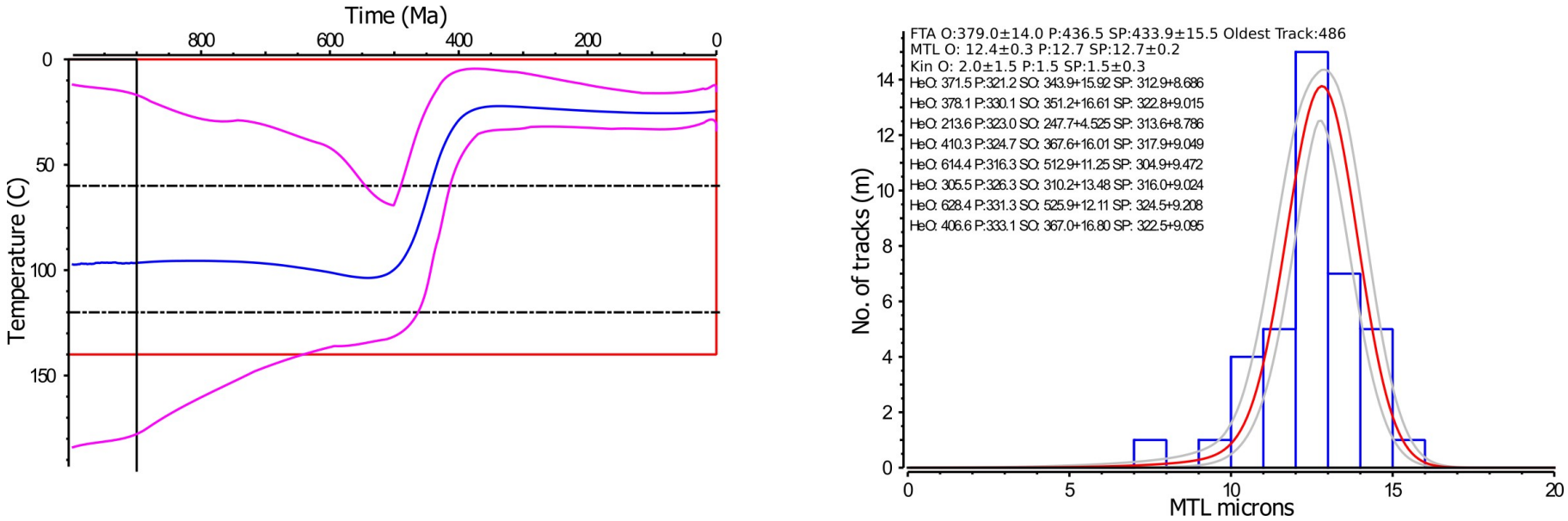

Figure S5: Additional thermal history models. Left hand figure: Blue line shows the expected model (i.e. average of all models weighted for their posterior probability); magenta lines indicate 95% credible intervals for the expected model. Red box indicates the prior information on temperature and time. Right hand figure: Histograms show the observed track-length distributions; red curve indicates the predicted track-length distributions, grey curves indicate 95% credible intervals (i.e. uncertainty) for track-length distribution prediction. FTA = fission track age, MTL = mean track length, Kin = kinetic parameter (i.e. Dpar), He = (U-Th)/He age; O = observed data, P = predicted data for the expected model, SO = sample observed (data resampled from the uncertainty range given on the observed age), SP = sample predicted (the mean and standard deviation of AHe ages for all models accepted during the inversion).

Figure S6: Denudation magnitudes.

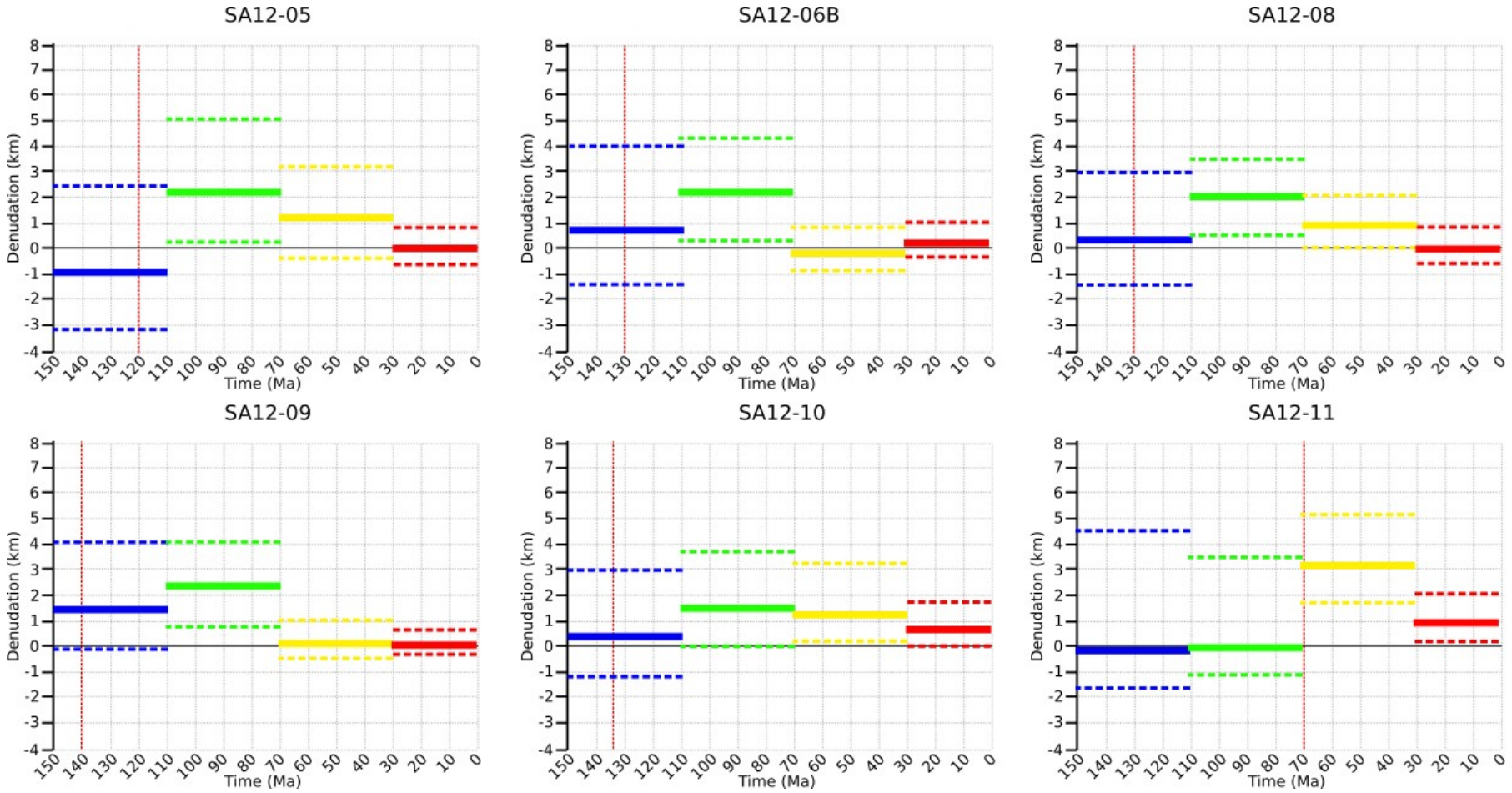

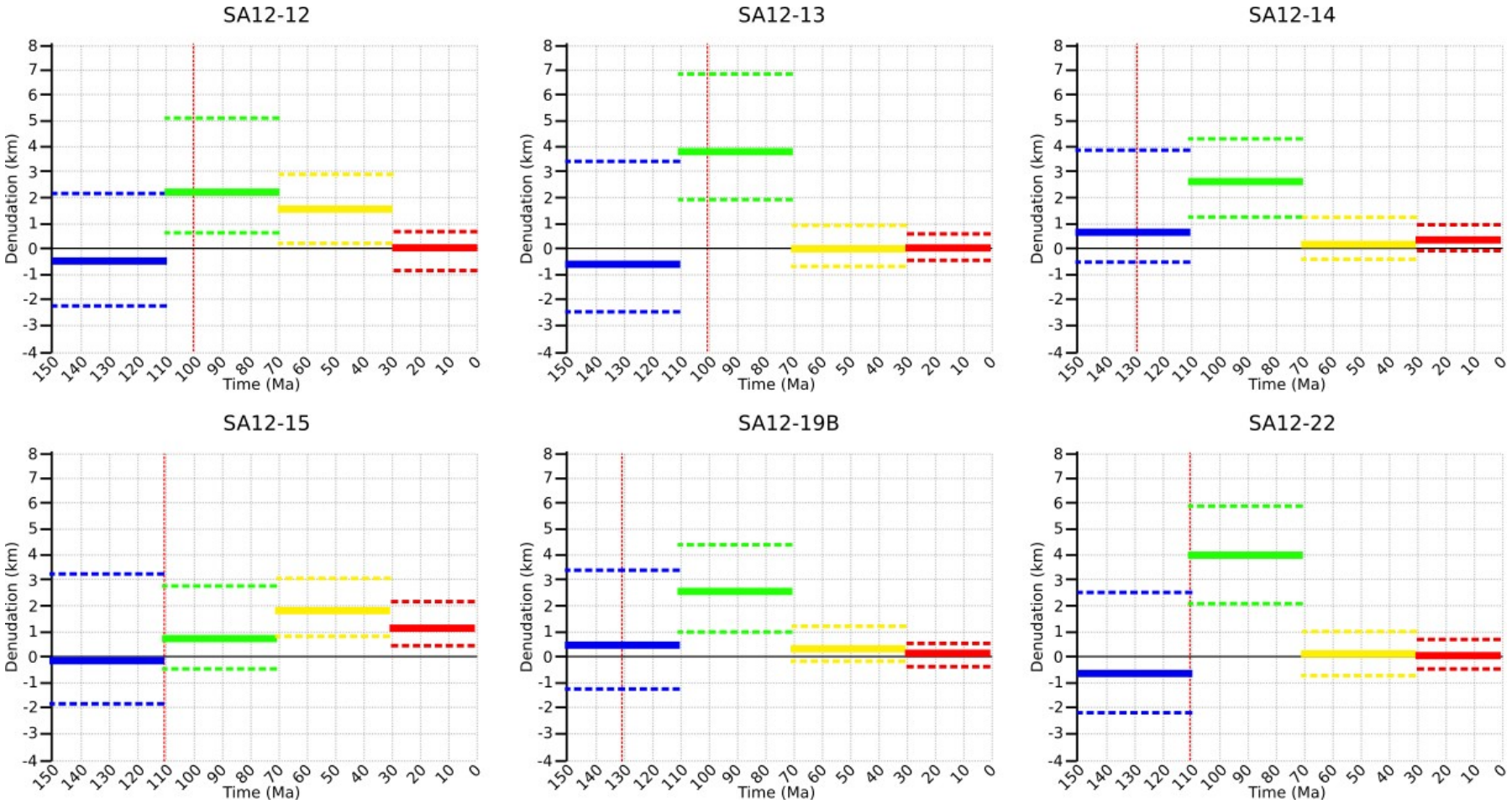
SA12-12
SA12-13
SA12-14
SA12-15
SA12-19B
SA12-22
Denudation (km)
Time (Ma)

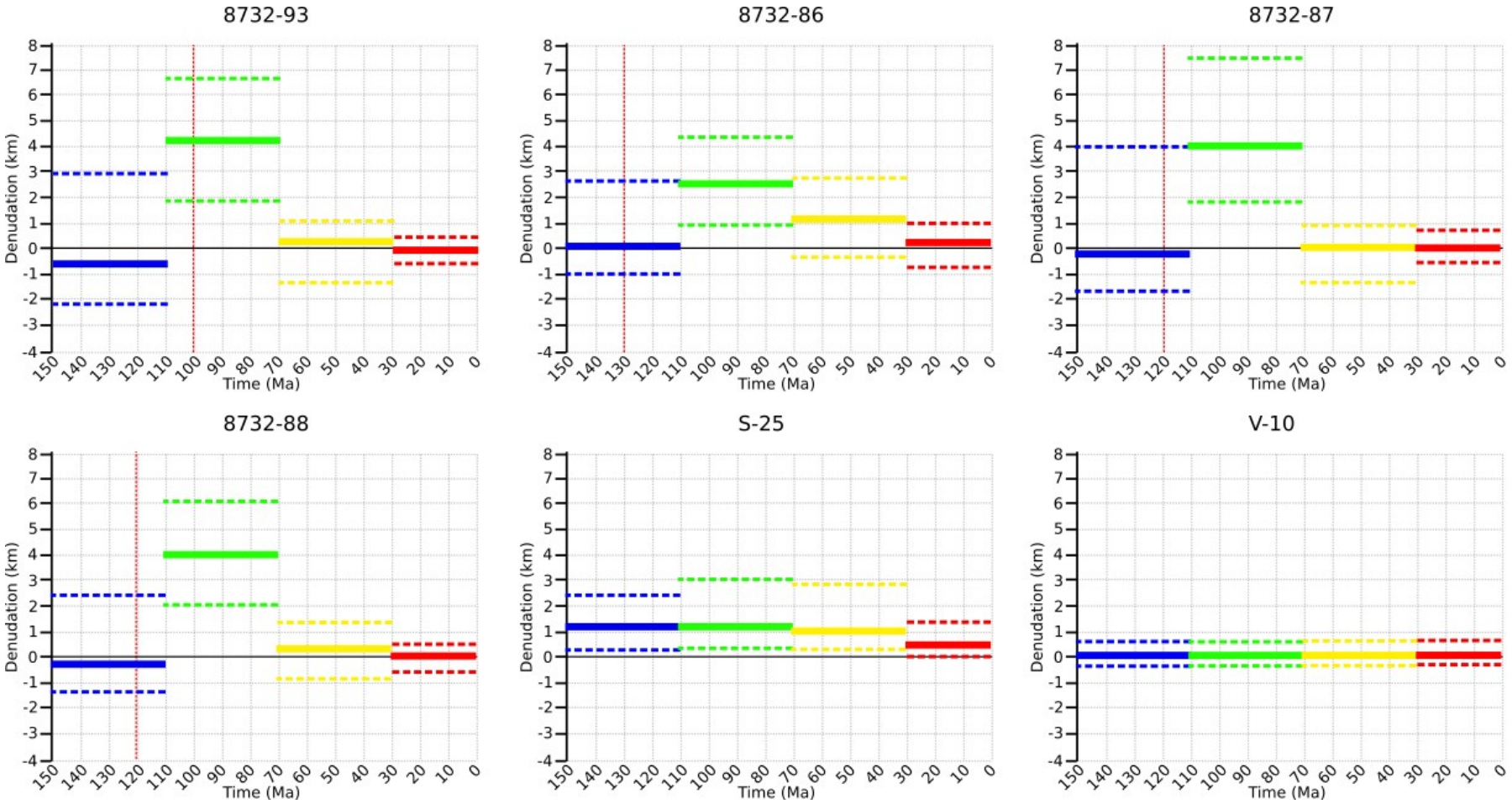
8732-93
8732-86
8732-87
8732-88
S-25
V-10
Denudation (km)
Time (Ma)

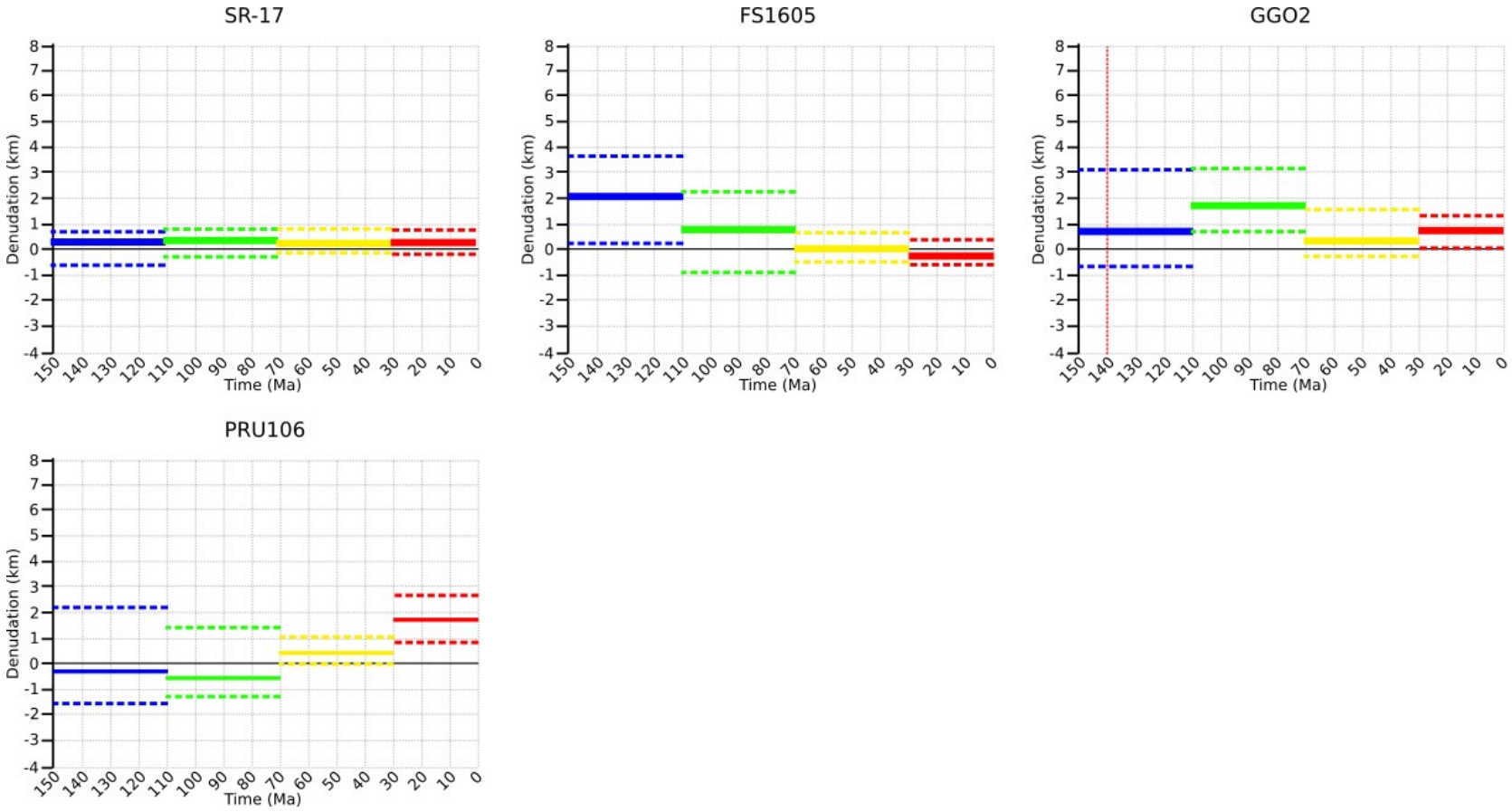

Figure S6: The expected thermal history for each sample has been used to constrain magnitudes of denudation over the intervals 150 – 110 (Blue), 110 – 70 (green), 70 – 30 (yellow) and 30 – 0 Ma (red). Denudation estimates were made by reading the change in temperature over the specified time interval from the expected thermal history model (blue t-T path in Figure S4) and dividing by an assumed geothermal gradient. In this case the geothermal gradient was assumed to be 25±°C/km. The uncertainty on temperature measurements was taken as the temperature of the 95% credible intervals at the start and end time of the specified interval. The uncertainties on denudation measurements were calculated using propagation of uncertainties on the geothermal gradient and temperature estimates. However, it should be noted that the 95% credible interval range represent a probability distribution and therefore the upper and lower uncertainty levels on denudation estimates should be considered as extreme values with a much lower probability than the estimated denudation using the expected model. The red dashed line represents the time when the model indicates that the sample was last at palaeo-temperatures of 100 – 120 °C. Before this time, models are entirely unconstrained due to earlier tracks having been annealed. Because of the additional uncertainty caused by this, the early Cretaceous (150 – 110 Ma) denudation map has been removed; however, for consistency the <150 Ma denudation history for all samples has been used in these plots.

TABLE S7

Long. (°)	Lat. (°)	Sample Name	Elev. (m)	Rock Type	Stratigraphic Age	Lithological Unit
22.20	-29.22	FS1605	843	Granite Breccia	Proterozoic	NMP
20.30	-28.36	GGO2	846	Granite	Proterozoic	NMP
19.52	-28.48	PRU 106	783	Navos Granite	Proterozoic	NMP
23.70	-29.15	SA12-05	1007	Granite dropstone (in Dwyka tillite)	Permian	Karoo Supergroup
23.14	-29.54	SA12-06b	1068	Bt. Gneiss (in Dwyka tillite)	Permian	Karoo Supergroup
22.31	-29.52	SA12-08	1039	hbl-bt-granite-augengneiss	Proterozoic	NMP
22.12	-29.40	SA12-09	995	Qtz-fdsp-bt Gneiss	Proterozoic	NMP
21.94	-29.36	SA12-10	1075	Porphyroblastic Qtz-fdsp-bt gneiss	Proterozoic	NMP
21.94	-29.24	SA12-11	1057	Coarse grained Porphyritic Granite	Proterozoic	NMP
21.63	-29.30	SA12-12	981	Bt-Qtz-Fsdp orthogneiss	Proterozoic	NMP
21.47	-29.28	SA12-13a	962	Paragneiss	Proterozoic	NMP
21.15	-29.35	SA12-14	797	Banded pelitic gneiss	Proterozoic	NMP
20.98	-29.42	SA12-15	884	Cg. Felsic Bt-Gneiss	Proterozoic	NMP
19.53	-29.34	SA12-19b	1034	Felsic qtz-fdsp-bt gneiss	Proterozoic	NMP
26.42	-26.63	V-10	1400	Granite	Archaean	Kaapvaal craton
25.25	-27.13	SR-17	1300	Granite	Archaean	Kaapvaal craton
26.08	-29.52	S-25	1450	Felspathic-sandstone	Lower Triassic	Upper Beaufort Group

TABLE S7: Lithological details for samples.